RESEARCH ARTICLE

VOLCANICA

Thermal remanence of the ~0.6 kya Rangitoto volcano eruption, Auckland Volcanic Field (New Zealand) inferred from self-potential and CO_2 flux measurements

Alutsyah Luthfian*[α,β], Anthony Finizola[γδ], Agnes Mazot[ε], Ludmila Adam[α], Rachel Gusset[γ], and Jennifer D. Eccles[α]

[α] School of Environment, The University of Auckland, Auckland, New Zealand.
[γ] Université de La Réunion, Laboratoire GéoSciences Réunion, Saint-Denis, La Réunion, France.
[δ] Université de Paris, Institut de physique du globe de Paris, CNRS, Paris, France.
[ε] GNS Science, Department of Volcanology, Wairakei Research Center, Taupō, New Zealand.
[β] Department of Geophysical Engineering, Institut Teknologi Sepuluh Nopember, Surabaya, Indonesia.

Submitted: 2024-06-10 | Accepted: 2025-02-27 | Published: 2025-04-30

Editor: Tom Pering | Typesetter: Gareth N. Fabbro

Abstract

Rangitoto volcano is the most recent (~0.6 kya) and voluminous volcano in New Zealand's Auckland Volcanic Field (AVF). In this study, we investigate the status of its hydrothermal system using a combination of self-potential (SP) and CO_2 gas flux measurements along the west-east Rangitoto–Motutapu main road. SP data revealed a "W"-shaped signal near the main crater, indicating an active hydrothermal system. In contrast, the CO_2 flux data showed diffuse emissions peaking 620 m east of the SP anomaly peak, suggesting they originated from different sources. The SP anomaly is likely due to a hydrothermal system heated by a shallow, cooling basalt body, and CO_2 emission is from deeper crustal or mantle sources. An SP electric potential offset was also detected at the Islington Bay Fault under the Rangitoto–Motutapu bridge without a corresponding CO_2 flux anomaly.

Résumé

Le volcan Rangitoto est le plus récent (~0,6 ka) et le plus volumineux du champ volcanique d'Auckland (AVF) en Nouvelle-Zélande. Dans cette étude, nous avons évalué l'activité de son système hydrothermal en combinant mesures de polarisation spontanée (PS) et de flux de CO_2 dans le sol le long de la route principale ouest-est Rangitoto–Motutapu. Les données PS ont révélé une forme en « W » à proximité du cratère principal, indiquant la présence d'un système hydrothermal actif. En revanche, les données de flux de CO_2 ont montré des émissions diffuses dont l'intensité maximum se situe à environ 620 m à l'est du pic de l'anomalie SP, suggérant qu'elles proviendraient de sources différentes. L'anomalie PS est probablement liée à un système hydrothermal chauffé par un corps basaltique peu profond se refroidissant, et les émissions de CO_2 proviendraient de sources crustales ou mantelliques plus profondes. Un décalage du potentiel électrique PS a également été observé au niveau de la faille d'Islington Bay sous le pont Rangitoto-Motutapu sans anomalie de flux de CO_2 correspondante.

Keywords: Auckland Volcanic Field; Rangitoto volcano; Thermal remanence; Hydrothermal system; Self-potential; Carbon dioxide.

1 Introduction

A hydrothermal system comprises advective processes that transport fluid from the heat source to the near surface [Norton and Knight 1977; Driesner and Geiger 2007]. The driver of a hydrothermal system can be cooling subsurface magma in a volcanic environment [Norton and Knight 1977; Norton 1984; Cathles et al. 1997] or fault-focused deep crustal fluids heated by the ambient geothermal gradient [Kühn and Stöfen 2005; Umeda et al. 2009]. Hence, hydrothermal systems can be found in diverse geological settings, e.g. calderas and polygenetic stratovolcanoes [Wohletz and Heiken 1992], small-volume volcanic fields [Aggarwal et al. 2003; Bolós et al. 2020; Revil et al. 2021], non-volcanic fore-arc domains [Umeda et al. 2009], or even tectonically stable intraplate regions [Kühn and Stöfen 2005].

Following the conclusion of a small-volume volcanic eruption, a hydrothermal system with meteoric recharge may be maintained on the newly formed volcanic edifice by the residual heat released from the cooling feeder dyke [e.g. Connor et al. 1997; Bolós et al. 2020]. When enough heat is available, this hydrothermal system may exhibit surface geothermal features such as fumaroles and steaming ground [Connor et al. 1997; Bolós et al. 2020] or trigger other hydrothermal eruptions that destroy the cone [Browne and Lawless 2001; Riggs and Duffield 2008; Lube et al. 2014; Stix and de Moor 2018]. However, once the hydrothermal system has cooled down and vegetation reoccupies any sites of past geothermal surface expressions, or if a hydrothermal system has always been a "blind" system, its existence is best detected geophysically [e.g. Aizawa et al. 2009; Hanson et al. 2014; Maza et al. 2018; Revil et al. 2023].

Fluid flow within the crust transports ions carrying electric charges, generating zones with varying ground electric potentials. The charge of the transported ions depends on the fluid's pH and the rock's zeta potential. Protons are generally transported when the fluid's pH exceeds ~4 and the rocks have negative zeta potentials [Wang and Revil 2010; Revil and Jardani 2013]. In contrast, negative ions are transported when

* alut525@aucklanduni.ac.nz

the fluid is highly acidic and the rocks have positive zeta potentials [Ishido and Mizutani 1981; Revil and Jardani 2013; Gresse et al. 2017]. However, the latter's situation is rarely found in geologically recent volcanoes [Aizawa 2008; Aizawa et al. 2008].

When the subsurface fluid's pH is neutral to basic and the rocks have negative zeta potentials, as groundwater flows down the flank of a volcano and the water table is further from the surface upslope, a decrease in ground electric potential will be observed with increasing elevation [Zlotnicki et al. 1998; Finizola et al. 2004; Linde et al. 2007; Onizawa et al. 2009; Revil et al. 2023]. In hydrothermal systems, thermally driven upflows [Zlotnicki et al. 1998; Ishido 2004; Revil et al. 2023] beneath the volcano can counter this trend and produce a localised zone of higher ground electric potential. Gravity-driven fluid flow through shallow conductive bodies beneath the volcano, such as clays from significant hydrothermal alteration, may also increase the ground electric potential [Ishido 2004; Onizawa et al. 2009]. If a volcano hosts, or ever hosted, a hydrothermal system, the ground electric potential curve may take a 'W' shape [Zlotnicki et al. 1998; Ishido 2004; Revil et al. 2023]. This shape comes from the superposition of 'V'-shaped topography-mirroring electrical potential variation due to downslope groundwater flow and localised 'Λ'-shaped area of higher electrical potential associated with thermally driven fluid upflows or shallow conductive bodies [Zlotnicki et al. 1998; Ishido 2004; Revil et al. 2023].

CO_2 gas comes from geologic and organic sources [Bennati et al. 2011]. Geologic sources include high-temperature 400–800 °C) reactions of carbonate minerals [Valley 1986; Harris et al. 1997; Bond et al. 2017], mantle sources [Weinlich et al. 1999], and degassing magma [Bennati et al. 2011]. Ascending CO_2 gas can follow a similar permeability pathway as hydrothermal fluids [Bennati et al. 2011]. Thus, a combination of self-potential and CO_2 flux explorations can provide information about high permeability zones atop a gas source at depth [Bennati et al. 2011].

Coupled self-potential and soil CO_2 gas flux measurements have been used to identify hydrothermal systems globally to reduce ambiguity. Its application to volcano-related hydrothermal systems has been presented, e.g. by Finizola et al. [2002] and Finizola et al. [2006, 2010] for Stromboli (Italy), Lewicki et al. [2003] for Masaya (Central America), and Byrdina et al. [2014] for Solfatara (Italy). This study presents the first-ever application of coupled self-potential and soil CO_2 gas flux measurements on Rangitoto volcano, a small-volume volcano within the Auckland Volcanic Field, to gain insight into the current state of its hydrothermal system. Despite their relatively small size, small-volume volcanoes may host hydrothermal systems for at least several decades following their formation (e.g. Jorullo [Hobson 1907] and Parícutin [Bolós et al. 2020], both in Mexico).

Rangitoto is the youngest (ca. 0.6 kya) and largest volcano in the intraplate Auckland Volcanic Field (AVF) in New Zealand [Figure 1; Needham et al. 2011; Hopkins et al. 2020]. This 6 × 5 km volcano rises to ~260 masl with a central group of scoria cones surrounded by a 2–3 km radius lava field [Needham et al. 2011]. Although Rangitoto scoria cones are highly oxidised [Kereszturi and Németh 2016], there is no systematic depth-related increase in alteration level [Linnell et al. 2016]. Next to Rangitoto to the east is the non-volcanic, 4 × 7 km Motutapu Island, rising to ~120 masl [Figure 1B; Kermode 1992; Edbrooke 2001]. A small canal separated the islands (Figure 1B).

2 Geology of the study area

Located at the Pacific and Indo-Australian tectonic plate boundary, New Zealand is a geologically dynamic area of volcanism and seismicity [Figure 1A, Spörli 1980]. The North Island's Quaternary volcanism can be divided into two groups: (1) arc volcanism related to the Hikurangi subduction margin, which includes large silicic calderas in the Taupō Volcanic Zone and voluminous stratovolcanoes such as Taranaki and Ruapehu [Figure 1A; Price et al. 1999], (2) small-volume intraplate volcanism distributed along the axis of the curvilinear Junction Magnetic Anomaly in the northern part of North Island [Figure 1A; Hopkins et al. 2020].

Intraplate small-volume volcanism in North Island commenced at ~10 Mya in the Northland Volcanic Fields [Figure 1A; Smith et al. 1993; Huang et al. 2000]. However, the locus of Northland Volcanic Fields activity is relatively fixed throughout its long lifetime [~10 Mya–40 kya; Smith et al. 1993; Hopkins et al. 2020] compared with the northward-migrating centres of intraplate volcanic fields south of it. These migrating centres were initiated at Ngatutura and Okete [~2.7–1.5 Mya; Hopkins et al. 2020], then continued to South Auckland [~1.6–0.5 Mya; Briggs et al. 1994; Hopkins et al. 2020], and since ~0.2 Mya is situated in the Auckland Volcanic Field [Figure 1A; Spörli and Eastwood 1997; Leonard et al. 2017; Hopkins et al. 2020].

2.1 Auckland Volcanic Field

The Auckland Volcanic Field (AVF) is a collection of 53 small-volume volcanoes distributed within the boundaries of Auckland's urban area, the major population centre of New Zealand [Figure 1B; Hopkins et al. 2020]. Volcanism in AVF commenced at ~193 kya and continued sporadically until the ~0.6 kya [Needham et al. 2011] Rangitoto eruption [Figure 1B; Leonard et al. 2017; Hopkins et al. 2020]. AVF rock composition varies from nephelinite to sub-alkaline basalt [McGee and Smith 2016; Hopkins et al. 2020] sourced from the upper mantle [Huang et al. 1997; McGee et al. 2013] and geochemically unrelated to the currently active Hikurangi subduction margin ~500 km east of AVF [Huang et al. 1997; 2000].

AVF volcanoes erupted over the surface of Plio-Quaternary unconsolidated sediments and Miocene Waitematā Group sandstone and mudstone sequences [Figure 1B; Kermode 1992; Edbrooke 2001]. These sedimentary units have been mapped to unconformably overlie the Mesozoic Waipapa metasedimentary basement, which outcrops outside the eastern boundary of AVF [Figure 1B; Kermode 1992; Edbrooke 2001]. In the central part of AVF, data from a 592 m-deep drill hole and seismic surveys [Edbrooke et al. 1998; Davy 2008] suggest the presence of the Eocene–Oligocene Te Kuiti Group sediments between the Waitematā Group sediments and the basement. Te Kuiti Group consists of calcareous sandstone, mudstone,

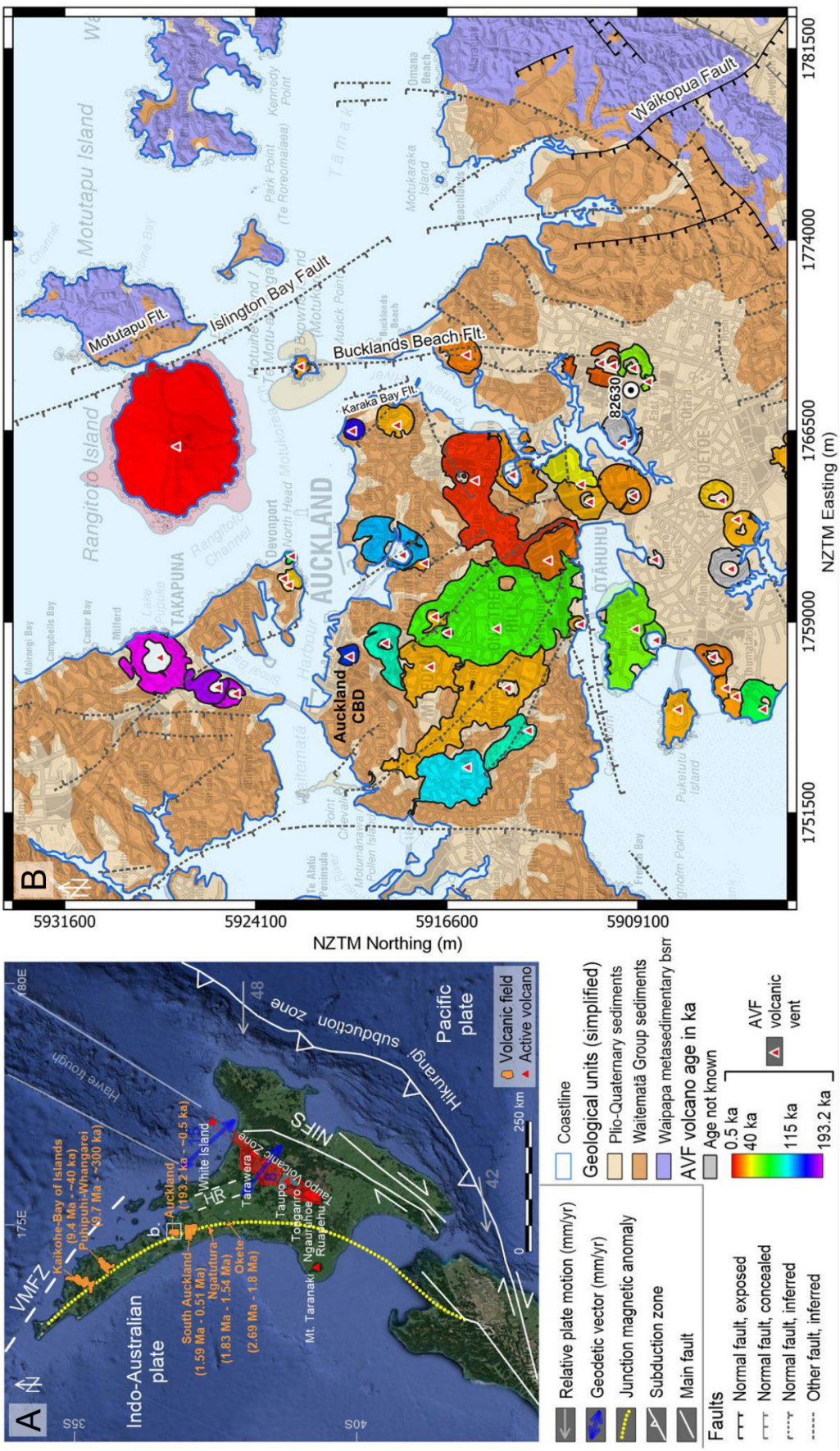

Figure 1: Tectonic setting and generalised geology of the Auckland Volcanic Field (AVF). [A] The tectonic setting of AVF, modified from Hopkins et al. [2020]. Geodetic vectors of extension [blue double arrows; Parson and Wright 1996; Wallace et al. 2004] and relative plate motion [grey single arrows; DeMets et al. 1994]. AVF is located over a potential Mesozoic terrane suture associated with the axis of Junction Magnetic Anomaly [yellow dashed line; Eccles et al. 2005], ~500 km west of the Hikurangi subduction margin (line with triangles on the upthrown block). HR: Hauraki Rift, NIFS: North Island Fault System [Beanland and Haines 1998], VMFZ: Vening Meinesz Fracture Zone. [B] Simplified geological map of the Auckland Volcanic Field [AVF; Edbrooke 2001; Heron 2023] overlying the New Zealand 1:50,000 topographic map by Land Information New Zealand (LINZ). Individual AVF vents with the age of their eruptive products [Leonard et al. 2017] and drill hole #82630 [penetrating the Te Kuiti Group; MBIE 2020, updated] are indicated. Fault (Flt.) traces and names are from Edbrooke [2001], Kenny et al. [2012], and Heron [2023].

and siltstone atop carbonaceous mudstone and coal layers [Edbrooke et al. 1998; Edbrooke 2001]. The combined sediment thickness under the AVF varies from ~0.9 km under the harbour near Auckland CBD to ~0.5 km in the west and east and 0.3 km in the southwest [Edbrooke et al. 1998; Kenny et al. 2012; Luthfian et al. 2023].

Statistical analyses found that AVF volcanic vents are aligned in NE–SW direction [e.g. Kear 1964; Von Veh and Németh 2009; Le Corvec et al. 2013; Bebbington 2015], approximately perpendicular to the dominant NW–SE strike of the mapped fault system [Figure 1B; Spörli and Kear 1989; Kenny et al. 2012; Le Corvec et al. 2013]. The general NE–SW trend of AVF vents may indicate structural influence on magma ascent by concealed ENE- to NE-trending faults cutting the basement and the overlying Miocene and older sediments [Giba et al. 2010; Jennings et al. 2023]. Another cause for the deviation of AVF vent alignment from the general fault trend is magma pathway modification by joints within the sedimentary units [Irwin 2009; Kenny et al. 2012].

While the Northland Volcanic Fields [Figure 1A Aggarwal et al. 2003] and some other global intraplate volcanic fields maintain the presence of surface thermal manifestations [e.g. Poblete Piedrabuena et al. 2016; Zhao et al. 2022], to date, no studies report such features associated with the AVF. CO_2 gas flux measurements over several discrete transects in the AVF and the subsequent analyses of AVF carbon dioxide gas samples show that AVF CO_2 gas emissions are biogenic and associated with urban land use, and values up to 203 $g\,m^{-2}\,d^{-1}$ were attributed to a non-volcanic source [Smid and Mazot 2012; Mazot et al. 2013]. The closest hydrothermal manifestation to the AVF is a non-volcanic hot spring at Waiwera, 35 km north of AVF, fed by ascending crustal fluids heated by the ambient geothermal gradient [Kühn and Stöfen 2005].

2.2 Rangitoto Volcano

Rangitoto is located 10 km east of Auckland's central business district in the Hauraki Gulf (Figure 2A). Its most recent known eruption was dated at ~1450 CE [Needham et al. 2011] and disrupted the life of local Māori [Figure 2B; Lowe et al. 2002]. Tephra from this eruption buried a Māori village on the northern shore of the neighbouring Motutapu Island, preserving cultural artefacts and footprints [Figure 2B; Nichol 1992; Lowe et al. 2002]. Rangitoto's duration of (non-continuous) eruptive activity is estimated to range from 30–60 yr [Needham et al. 2011], 150–450 yr [Allington et al. 2023], to 1000 yr [Shane et al. 2013]. Rangitoto has erupted at least ~0.7 km^3 of material, comprising 41 % of the total erupted volume in the AVF [dense-rock equivalent volumes; Kereszturi et al. 2013]. This volume is divided into a ~0.05 km^3 central steep side complex of scoria cones and a ~0.65 km^3 lava field [Figure 2C; Kereszturi et al. 2013]. The lava field radiates 2–3 km from the scoria cone complex like a shield and dips seaward at 4°–12° [Figure 2C; Needham et al. 2011].

Evidence from a 148 m-deep drill hole (RANG in Figure 2) and foraminiferal fossils hint that the first eruptions of Rangitoto occurred in a shallow marine setting [Linnell et al. 2016; Hayward et al. 2022]. The latter phases of the eruption saw an increasing magma supply, with which the volcano could build a subaerial scoria cone and an extensive lava field [Figure 2; Smith and Németh 2017]. Gravity and magnetic modelling of Rangitoto indicates a potential shallow (<300 m) basaltic body beneath the Rangitoto scoria cone [Luthfian et al. 2023]. Currently, no active hydrothermal manifestations are observed on the island.

2.3 Motutapu Island

To the east of the Rangitoto volcano is the non-volcanic Motutapu Island (Figure 3C, 3D). The western part of this island is covered by 90 m thick Waitematā Group sediments, which thins eastward to reveal the Waipapa metasedimentary basement [Figure 2C; Luthfian et al. 2023]. Several basement faults have been mapped on Motutapu Island, with the NW-trending Motutapu Fault and Islington Bay Fault as the most prominent ones [Figure 2C; Mayer 1968; Kenny et al. 2012; Luthfian et al. 2023]. The Motutapu Fault is estimated to have at least ~90 m vertical displacement [Mayer 1968]. Gravity modelling estimated that the Islington Bay Fault has a 300 ± 50 m vertical displacement [Luthfian et al. 2023]. Extrapolation of Islington Bay Fault to depth could link this structure with a collocated shear wave speed discontinuity at 2–10 km depth described by Ensing et al. [2022], signifying a potential linkage to deeper crustal structures. Several shallow (≤10 km deep) earthquakes have been generated under Motutapu Island [GNS Science 1970, updated], suggesting that these crustal structures can still be reactivated. No evidence of hydrothermal manifestations on Motutapu has been reported. Nevertheless, we can investigate permeability contrasts and the presence of hydrothermal fluids and understand how crustal structures contribute to the fluid flow under Motutapu Island using the self-potential and gas flux measurements, as in Bond et al. [2017] and Revil et al. [2023].

3 Methodology

3.1 Self-potential method

The self-potential (SP) geophysical method indirectly measures ground electric potential by looping a series of electric potential difference data to an equipotential surface or any other point [Revil et al. 2023]. Our work measured electric potential differences every 20 m along the Rangitoto-Motutapu main road (Figure 3) by a roving electrode connected to a fixed reference station spaced every 100 m. The electrodes are a pair of non-polarising Cu–$CuSO_4$ electrodes assembled according to Revil et al. [2023]. Ground contact during the survey (28–30 July 2023) was good as the surface of Rangitoto and Motutapu was still wet from several rainy days previously (25–27 July 2023). Electric potential difference is measured with a calibrated high-impedance (100 MΩ) voltmeter with an uncertainty of 0.5 mV. Horizontal data position is recorded by a handheld GPS with 1–2 m horizontal uncertainty, while the data elevation is sampled from the Auckland LiDAR 1 m horizontal resolution with 0.2 m vertical uncertainty [Land Information New Zealand 2018].

We convert the potential difference into the SP electric potential values (V_{SP}, in millivolts) using the following formula

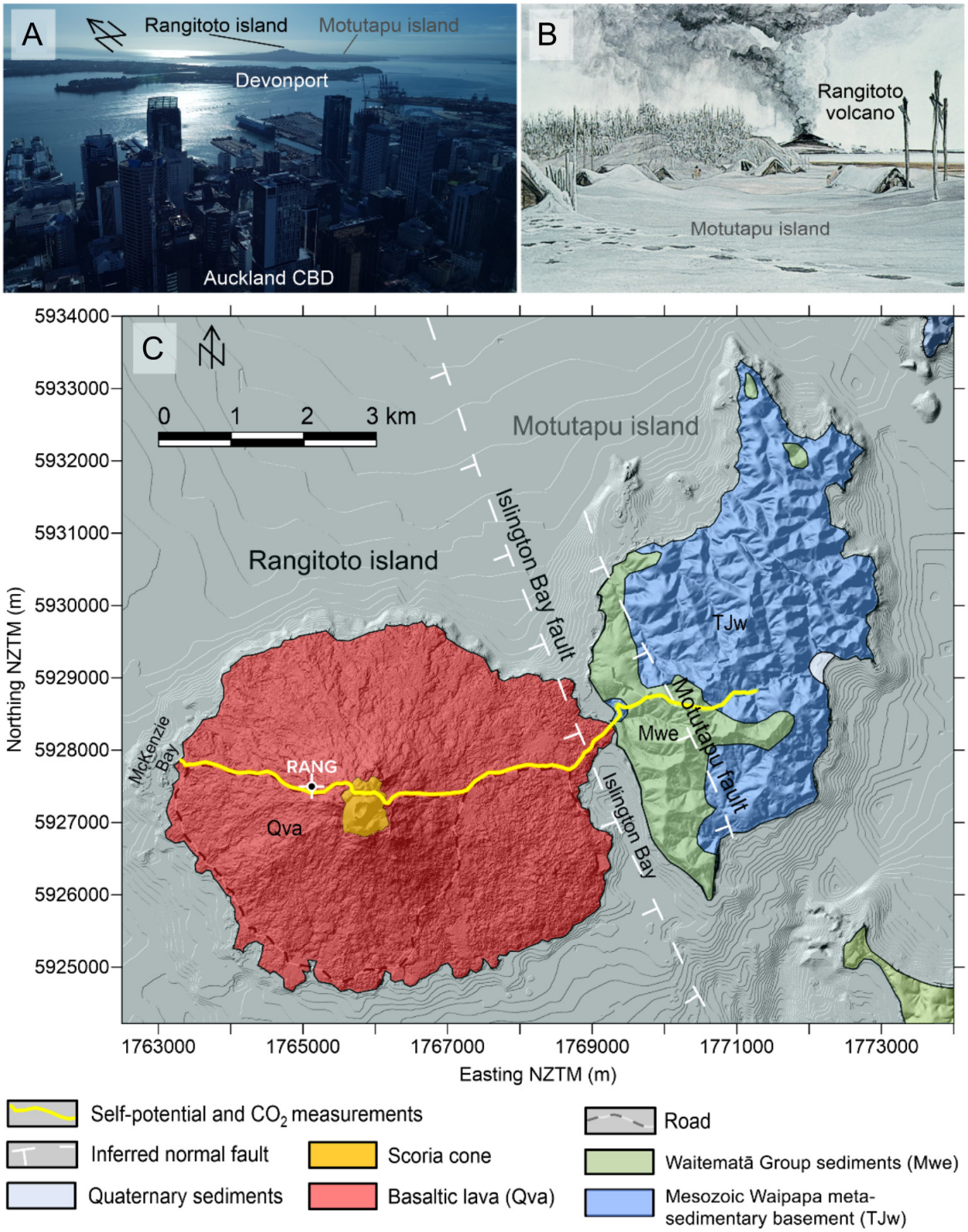

Figure 2: [A] Rangitoto Island seen from the Sky Tower, Auckland CBD. Motutapu Island is located behind Rangitoto. [B] Artistic rendering of the Rangitoto eruption affecting a local Māori fishing village on Motutapu Island. Painting by Chris Gaskin [1990]. [C] Rangitoto geological map [adapted from Kenny et al. 2012; Heron 2023] draped over the shaded relief map from NIWA [Mackay et al. 2012], with the self-potential and gas flux measurement transect (yellow line). Abbreviations indicate the surface geological unit associations (TJw: Mesozoic Waipapa metasedimentary basement, Mwe: Waitematā Group sediments, Qva: basaltic lava field). Location of drill hole "RANG" [Linnell et al. 2016] is indicated with "+".

[after Revil et al. 2023].

$$V_{SP} = V_{meas} + V_{ref} - V_{loopcor} \quad (1)$$

In the equation above, V_{meas} is the measured potential difference, V_{ref} is the potential difference between the roving and a reference station, and $V_{loopcor}$ is the loop correction gained by closing the SP transect to the sea surface. The reference station (0 mV) reading was taken a few m (horizontal distance) from the sea at McKenzie Bay, where the first fixed electrodes were located (first point). The loop correction was performed at Islington Bay, where the potential was measured a few m (horizontal distance) from the sea. Due to algebraic operation, the uncertainty of the SP electric potential values is 1 mV.

3.2 CO_2 gas flux measurement

We measure the soil CO_2 flux using the accumulation chamber technique, a passive geochemical method for measuring the flux of diffuse CO_2 emission from soil [Chiodini et al. 1998]. We use a portable gas flux meter developed by West Systems S.r.l, fitted with an infrared (IR) spectrometer (LICOR 850 CO_2 detector, with a full scale of the detector used of 20 000 ppm, with an accuracy <1.5 % of reading and zero drift <0.15 ppm °C^{-1}), a Type-B accumulation chamber (internal volume 0.006 m^3), and a smartphone for real-time data visualisation and quality control. The IR spectrometer was calibrated with gas standards before fieldwork. To start the measurement, we secure the accumulation chamber on top of the soil to allow gases to collect in the accumulation chamber. The gas-air mixture in the accumulation chamber is continuously pumped and analysed by the IR spectrometer. Data from the spectrometer is then sent to the smartphone, which plots the concentration-time curve. Wherever the soil emits CO_2 gas, the concentration-time curve will show a clear linear trend with a positive slope. The slope of concentration-time curve ($\frac{dc}{dt}$, in ppm s^{-1}) is proportional to and can be converted to daily soil CO_2 flux (F_{CO_2}, in g m^{-2} d^{-1}) using the following equation [Mazot et al. 2013].

$$F_{CO_2} = k \times \frac{V}{A} \times \frac{T_0}{T} \times \frac{P}{P_0} \times \frac{dc}{dt} \quad (2)$$

In Equation 2, k is a constant to convert parts per million per second (ppm s^{-1}) to g m^{-2} d^{-1} and is equal to 155.87 m^{-3}, V is the accumulation chamber volume (in m^3), A is the area of the accumulation chamber base (in m^2), T_0 and P_0 are standard temperature and pressure (298 K and 101.3 kPa, respectively), T is the measured temperature (in K), P is the measured air pressure in kPa [Smid and Mazot 2012; Mazot et al. 2013].

A gas flux measurement is stopped when a linear and unambiguous trend appears in the concentration-time curve, which usually happens 1 to 2 minutes after the measurement starts. The sensitivity limit of our portable gas flux meter is 0.4 ppm s^{-1} [West Systems 2020], and any measurement with a concentration–time curve slope of <0.4 ppm s^{-1} is recorded as zero. At the start of every measurement, we ensure that the gas flux meter system cleans itself of gas remnants from the last measurement, which usually takes the first 10 s of the next measurement. To ensure we acquire geological CO_2 gas flux anomalies, we strive to measure gas flux away from organic remains and plants to minimise ambiguity. This was possible for most of the transect, but there is a segment on Motutapu Island where we could not avoid grass and a muddy road, and we recorded this accordingly (Figure 3). Weather conditions during the three days of CO_2 flux measurement were stable, and no weather event influenced the acquired CO_2 flux data. Although rainy days occurred before the fieldwork—potentially increasing soil water content, which may reduce measured CO_2 flux [Hashimoto and Komatsu 2006]—this is less of a concern since we are primarily focused on CO_2 flux anomalies arising from structural features, determined by locating flux intensity changes and looking at the overall pattern of the anomaly across different parts of the transect rather than individual absolute values.

We are aware that self-potential and gas flux signals may change through time [e.g. Laiolo et al. 2016; MacAllister et al. 2016], and to guarantee that the two data can be interpreted jointly, we conducted the gas flux measurements in tandem with the self-potential work (Figure 3). A total of 463 self-potential and 463 CO_2 degassing measurements were performed contemporaneously, each 20 m along a profile 9240 m long, from McKenzie Bay to the west on Rangitoto Island up to the middle of Motutapu Island to the east (Figure 3C).

4 Results

4.1 SP and CO_2 gas flux curves of Rangitoto and Motutapu

The SP electric potential curve (Figure 4) of Rangitoto-Motutapu is 'W'-shaped over Rangitoto Island, while it is nearly flat over Motutapu Island. The 'W'-shaped SP curve over Rangitoto is similar to those observed on volcanoes with a hydrothermal system, whether manifesting at the surface [e.g. Zlotnicki et al. 1998; Finizola et al. 2004; Onizawa et al. 2009] or concealed [e.g. Aizawa et al. 2005; Aizawa 2008; Revil et al. 2011; Gresse et al. 2021]. The west (segment A) and east (segments D–F) arms of Rangitoto's 'W'-shaped SP curve correlate negatively to the topography (Figure 4). Meanwhile, the central 'Λ' peak of the Rangitoto SP curve (segment B) has slopes positively correlated with the topography (Figure 4). A section with a relatively constant SP value is observed in segment C (Figure 4).

Due to the differences in geology and vegetation between Rangitoto and Motutapu, we divided the analyses of the CO_2 flux data for the 9240 m long profile into two parts: (1) the Rangitoto section from 0–6780 m and (2) the Motutapu section from 6800–9240 m. On the Rangitoto section of the profile, from the 340 CO_2 flux measurements, 263 (77.4 %) are below the detection limit, and the average on the measurable CO_2 flux values is 6.6 g m^{-2} d^{-1}, with the highest value of 24.3 g m^{-2} d^{-1}. On the Motutapu section of the profile, from the 123 CO_2 flux measurements, 93 (73.2 %) are below the detection limit, and the average on the measurable CO_2 flux values is 10.0 g m^{-2} d^{-1}, with the highest value of 34.5 g m^{-2} d^{-1}. These statistical descriptions are consistent with the 5-data moving average window in Figure 4, showing a generally higher CO_2 amplitude anomaly on Motutapu Island than on Rangitoto Island. It is important to note that

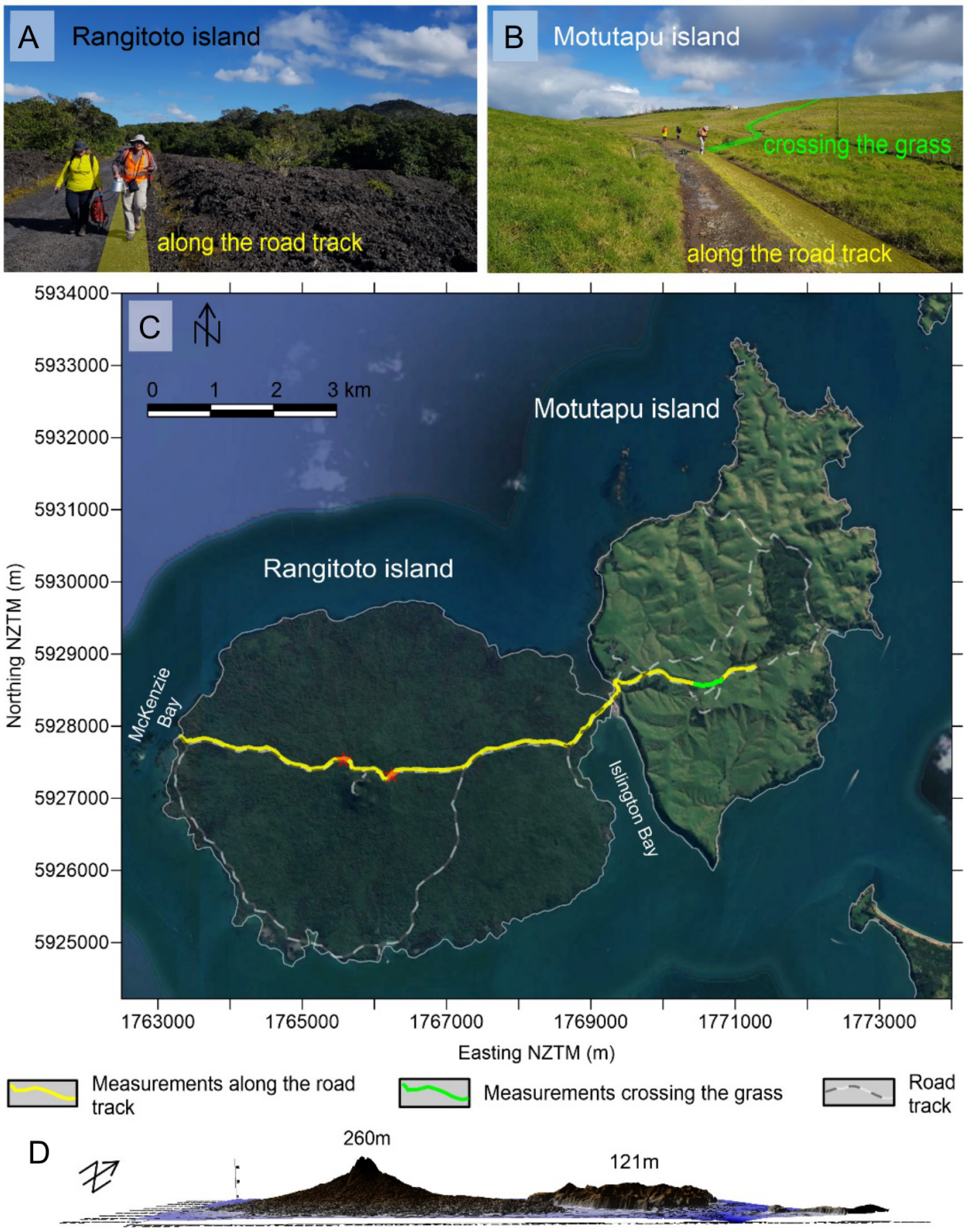

Figure 3: [A] A joint self-potential (SP) and CO_2 measurement site over the aa lava flow on Rangitoto Island. [B] A section on Motutapu Island where a high CO_2 gas flux is detected associated with grasses, mud, and other organic matter. [C] The location of along-road (yellow and orange lines) and on-grass (green line) measurement transect on the Rangitoto and Motutapu islands satellite imagery. While the tone suggests extensive vegetation on Rangitoto, field observations reveal a mix of open black lava field and mature and regenerating vegetations. Red stars near the Rangitoto summit mark the transition between negative to positive SP/elevation gradient (the two minima of the "W" shape SP signal; see text). [D] Rangitoto and Motutapu Islands elevation variation viewed from the southeast.

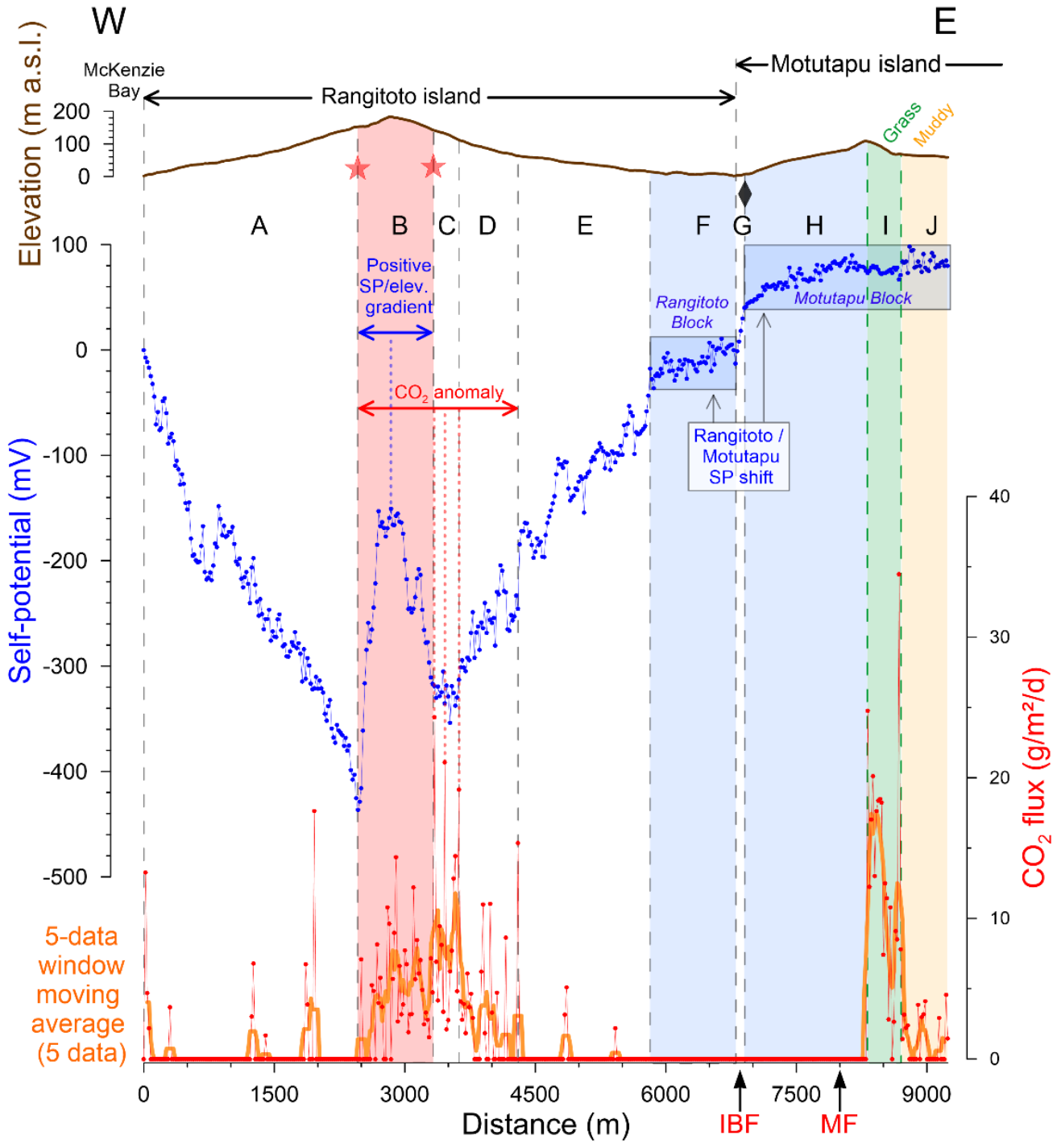

Figure 4: Profile of the Rangitoto-Motutapu elevation (topmost), SP electric potential (middle, blue), and CO_2 gas flux (bottom, red) over the measurement transect. Segments (or sections) are marked by letters and colours. Segments A and C–F are on Rangitoto volcano flanks, and section B is on Rangitoto scoria cone where the maximum SP anomaly occurs. A significant CO_2 gas flux anomaly is observed on segments B–C–D. Red stars near the Rangitoto summit mark the transition between negative to positive correlation of SP and topography (the two minima of the "W" shape SP signal; same symbol as in Figure 3). Segments F and H–J are parts where the horizontal gradient of the SP curve becomes gentler and are termed "blocks". Rangitoto Block (segment F) is separated from Motutapu Block (segments H–J) by a ~60 mV offset (segment G) associated with the Islington Bay Fault (IBF). Grassy (segment I) and muddy road (segment J) sections on Motutapu Island is indicated and correlate to CO_2 anomalies. MF: Motutapu Fault. Black diamond: location of the Islington Bay Fault below the topography.

the maxima of CO_2 flux values encountered on both islands are a few orders of magnitude lower than that on active volcanoes such as La Fossa of Vulcano [up to 14 000 g m^{-2} d^{-1}; Revil et al. 2008], Vesuvius [up to 1500 g m^{-2} d^{-1}; Granieri et al. 2010], Solfatara [up to 20 000 g m^{-2} d^{-1}; Granieri et al. 2010], or even the recently erupted Parícutin scoria cone [up to 180 g m^{-2} d^{-1}; Jácome-Paz et al. 2022].

On Rangitoto island, although the CO_2 flux displays high-frequency spatial variations, the general shape of the anomaly approximates the Gaussian bell curve (see the 5-data window moving average in Figure 4). The central part of the anomaly, from 2860 m up to 3780 m (920 m long), is characterised by a succession of CO_2 flux values between 1.5 and 24.3 g m^{-2} d^{-1}, without any data below the detection limit. The maximum lateral extension of this CO_2 flux anomalous area encompasses the Rangitoto's summit area and the upper eastern flank. The western and eastern flanks of this peak feature a gradual decrease of CO_2 flux values with increasing frequency of data below detection limits for 360 m and 520 m, respectively, before entering zones of dominantly flat CO_2 flux signal before the 2500 m and after the 4300 m (segments B–D, Figure 4). Vegetation covers the Rangitoto flank unevenly (Figure 3) and uncorrelated with the CO_2 gas flux anomaly peaks. The centre of this CO_2 gas flux anomaly is shifted ~620 m to the east of the SP curve central 'Λ' peak (Figure 4). Thus, the western part of the elevated CO_2 gas flux zone overlaps with the central peak of the SP curve (segment B) and flat segment C, while its eastern part overlaps with the east arm of Rangitoto's 'W'-shaped SP curve (segment D, Figure 4). Localised (<50 m) areas with <20 g m^{-2} d^{-1} CO_2 gas flux were also observed in segments A and E (Figure 4).

The gradient of the SP curve with horizontal distance over Rangitoto is generally steep, except on the easternmost 1 km of Rangitoto Island, where it becomes gentler and matches a nearly flat SP gradient over Motutapu Island (Figure 4). The parts with a gentler SP horizontal gradient are arbitrarily termed Rangitoto (segment F) and Motutapu (segments H–J) blocks to distinguish them from parts with a steeper horizontal SP gradient, which forms the bulk of the 'W'-shaped curve over the Rangitoto edifice (Figure 4). Motutapu Block is offset by about +60 mV from the Rangitoto Block in segment G without any corresponding increase in CO_2 gas flux (Figure 4). However, a relatively high CO_2 gas flux (up to ~20 g m^{-2} d^{-1}) is detected over a grassy section on Motutapu without an accompanying SP signature (segment I; Figure 4). This value is consistent with CO_2 gas flux rate observed over grasslands in other parts of the world [Raich and Tüfekçioğlu 2000; Hu et al. 2001]. Immediately east of this grassy section is a segment located on a muddy road with a noisy SP signal and up to ~5 g m^{-2} d^{-1} CO_2 gas flux (segment J; Figure 4).

4.2 Analysis of the Rangitoto SP curve

Suppose we have elevation Z and SP electric potential V at several x points. We can fit the following linear model (Equation 3, with the ε as an arbitrary fitting intercept) to a set of x points in a segment with a constant C_e [Finizola et al. 2004].

$$Z(x) = [C_e \times V(x)] + \varepsilon \quad (3)$$

With this concept, we can segment the Rangitoto SP curve according to their C_e, as in Figure 5. C_e-based segmentation of the Rangitoto SP curve shows mirroring western and eastern flanks' C_e segments. Each mirrored segment has the same C_e signs and is indicated with matching colours in Figure 5 (e.g. W2 versus E2, W4 versus E4, W7 versus E7).

Segments with ≤0 mV m^{-1} C_e on the western (W1–W4) and eastern (E1–E4) flanks of Rangitoto represent its hydrogeological zones, where the groundwater flows down the flank, and the water table is potentially further from the surface upslope [Figure 5A; Linde et al. 2007; Richards et al. 2010]. The C_e values within Rangitoto's hydrogeological zones W1–W3 and E1–E3 range between −1.7 and −6.1 mV m^{-1} (Figure 5A, 5B). However, the hydrogeological zones closest to the Rangitoto summit, W4 and E4, have a C_e of ~0 mV m^{-1} before changing their sign to positive C_e values in zones W5 and E5 (Figure 5A, 5B). As we enter segments W5 and E5 toward the Rangitoto summit, two short (≤~100 m) segments with negative C_e values, W6 and E6, interrupt this summit-ward positive C_e value trend at the base of the Rangitoto scoria cones (Figure 5A, 5B). Then, C_e values become positive again before they flatten ($C_e \approx 0$ mV m^{-1}) on the highest segments (W8 and E8; Figure 5A, 5B).

5 Discussion

5.1 Rangitoto Hydrothermal System

Although ~0.6 kya has passed since the Rangitoto eruption [Needham et al. 2011], SP data collected over the volcano displays a signature 'W'-shaped curve with the 'Λ' part encompassing and slightly exceeding the scoria cone region (Figures 4 and 5). The 'W' arms with $C_e \leq 0$ mV m^{-1} over the western and eastern Rangitoto flanks (segments A, D–E; Figure 4) are associated with hydrogeological zones where the aquifer is replenished by meteoric water and possibly sits deeper as elevation increases. Meanwhile, the 'Λ' section of the Rangitoto SP curve (segment B; Figure 4) is a potential hydrothermal zone associated with a shallow hydrothermal fluid upflow under the Rangitoto cone.

Materials with high electrical conductivity, e.g. clays, could produce a high SP value. Two potential alternatives exist: (1) the Rangitoto eruption substrate made of shallow marine muds or pre-Rangitoto tuff ring/maar [Hayward et al. 2022] and (2) Rangitoto scoria cone alteration products. The former are unlikely since the pre-eruptive strata would be broadly distributed at depth rather than spatially localised within the central Rangitoto edifice [Hayward 2022; Hayward et al. 2022]. Regarding mineral alteration of the Rangitoto scoria, although the Rangitoto cone is highly oxidised, none of the quarried AVF scoria cones, all significantly older than Rangitoto, has been known to develop an intra-cone thick clay layer [e.g. ~30 kya Three Kings and ~20 kya Mt Smart scoria cones; Hayward and Jamieson 2019; Hopkins et al. 2020]. Volcanic materials encountered in the Rangitoto drill hole also lack alteration [Linnell et al. 2016]. Thus, the hydrothermal system hypothesis is the most plausible explanation for the observed 'W'-shaped SP curve on Rangitoto (Figure 4). With this understanding in mind, we can now interpret the near-surface

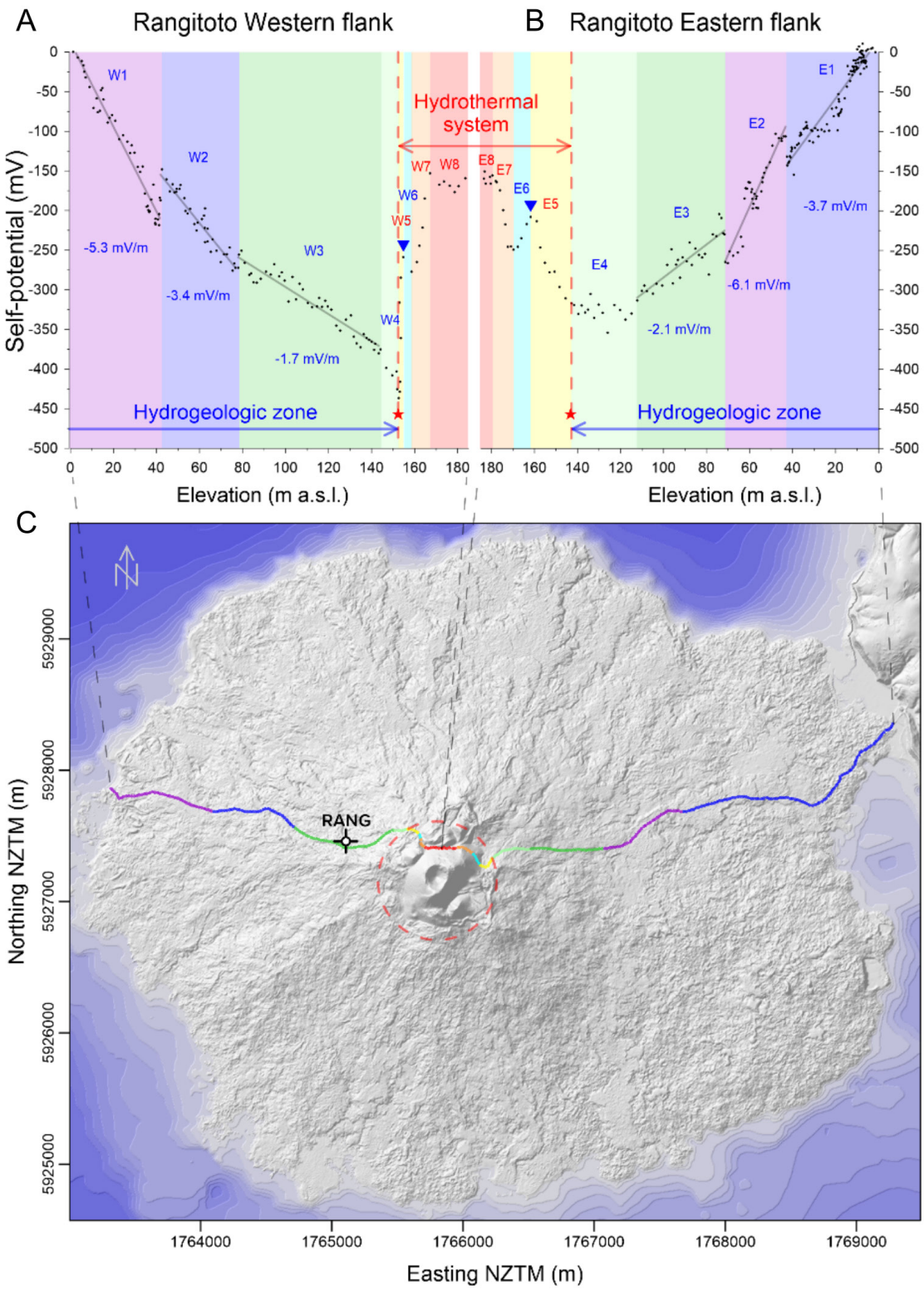

Figure 5: Segmenting the Rangitoto SP curve based on the SP to elevation gradient (C_e) to differentiate the hydrogeological (negative C_e) and hydrothermal (positive C_e) zones on the western [A] and eastern [B] sides of Rangitoto. The segments are labelled with W/E[number], with W and E denoting the sides (western/eastern) where the segments are located. Colours emphasise pairs of mirroring W and E segments. Red stars near the Rangitoto summit mark the transition between negative to positive SP/elevation gradient (the two minima of the "W" shape SP signal; same symbol as in Figures 4 and 5). [C] Location of the segments described in [A] and [B] laid over the Rangitoto shaded relief map. The extent of the Rangitoto hydrothermal system (red dashed circle) encompasses and exceeds the Rangitoto scoria cone. The sea is coloured with shades of blue, with darker shades signifying deeper depths. Location of drill hole "RANG" [Linnell et al. 2016] is indicated with a "+".

aspects of a Rangitoto hydrothermal system indicated by the pattern of SP and C_e values inside the hydrothermal zone.

Inside the Rangitoto hydrothermal zone, at the western and eastern base of Rangitoto scoria cones, a short downward bend in the SP curve can be observed within segment B (Figure 4), correlated with short (≤100 m) negative C_e segments, W6 and E6 (Figure 5). We can decompose this bent SP curve into two independent, single-amplitude SP curves of different wavelengths: one is shorter (~1 km wavelength) with a negative amplitude, and the other is longer (~1.4 km wavelength) with a positive amplitude (Figure 6B). The longer, positive-amplitude SP curve is associated with the upward hydrothermal fluid flow, whilst the shorter, negative-amplitude SP wave is most likely associated with near-surface, downward meteoric fluids percolation influenced by the highest permeable medium constituting the scoria cones [similar superimposition of short wavelength negative SP minima on higher wavelength positive anomalies have been already observed on the summit part of Stromboli volcano; Finizola et al. 2003]. The downward bends in the hydrothermal zone SP curve reflect segments where the meteoric fluid flow signature overprints on the deeper potential difference induced by the hydrothermal upflow (Figure 6B). Short negative C_e segments (W6 and E6), which coincide with the SP curve bends at the base of Rangitoto scoria cones, are expected as they are located close to contacts between scoria and lava (Figure 6A), two lithologies that have a contrasting permeability [≥50 % for scoria versus ≤50 % for lava; Saar and Manga 1999], porosity [greater for scoria cones; Kereszturi et al. 2013] and thus electrokinetic properties [Lénat 2007].

There are two possible drivers for the Rangitoto scoria cones' hydrothermal system: a shallow heat source under the Rangitoto scoria cone (Figure 7) or deep crustal fluids [as in Waiwera; Kühn and Stöfen 2005] seeping through the pathway opened or exploited by Rangitoto magma. From the more localised spatial extent of the SP central peak compared to the CO_2 gas flux one, both scenarios seem possible since the CO_2 gas is expected to be capable of percolating through the less permeable lava than water (Figure 4). However, if this was the case, the spread of the CO_2 central peak should be symmetric about the axis of the more restricted SP peak since the CO_2 gas will also utilise the same more permeable pathway as the hydrothermal water [e.g. Finizola et al. 2003]. Even if the SP peak were "muted" atop the lava field, the C_e value would help indicate the centre of subsurface fluid upflow [e.g. Lénat 2007]. All these are not observed on Rangitoto, where the SP and C_e peaks are offset ~620 m west of the CO_2 gas flux peak (Figure 4), suggesting that the driver of hydrothermal processes associated with the central Rangitoto SP peak differs from the one associated with the CO_2 gas flux anomaly. The Rangitoto SP central peak is confined within the Rangitoto scoria cones, suggesting a hydrothermal heat source likely linked with the latest [~0.6 kya; Needham et al. 2011] Rangitoto activities, e.g. a cooling basalt body at <300 m depth [Figures 4 and 7; Luthfian et al. 2023]. Cooling near-surface igneous bodies have also been proposed for several hydrothermal systems associated with small-volume volcanic fields globally, e.g. Surtsey [Jakobsson and Moore 1986] and Paricutín [Jácome-Paz et al. 2022].

5.2 Source of Rangitoto diffuse CO_2 emission

The range of Rangitoto CO_2 gas flux anomaly at its central peak is relatively low (1.5–24.3 g m^{-2} d^{-1}; Figure 4) compared to elsewhere in the Auckland Volcanic Field [up to 203 g m^{-2} d^{-1}; Mazot et al. 2013], recently active Parícutin scoria cone [up to 180 g m^{-2} d^{-1}; Jácome-Paz et al. 2022], or other volcanic regions globally [e.g. Vesuvius, up to 1.500 g m^{-2} d^{-1}; Granieri et al. 2010]. While high CO_2 flux values often suggest a stronger source, it is essential to note that in volcanic contexts, the origin of a CO_2 anomaly cannot be directly inferred from flux intensity alone. Rather, the observed flux depends on a combination of factors, including the strength of the degassing source, the permeability of subsurface structures linking the source to the surface, and any sealing effects within hydrothermal systems [Finizola et al. 2003; 2004; Revil et al. 2004; 2019].

To address the possibility of a biogenic source, we examined the distribution and type of vegetation across Rangitoto Island using satellite imagery (Figure 3C) and a map from Julian [1992]. CO_2 measurements were taken along a clean gravel road that passes through varied vegetation zones, including forest patches on the lava field and scrubland on the scoria cone [see Figure 3A and Julian 1992]. If a shallow, biogenic source were responsible for the observed CO_2 anomalies, we would expect multiple CO_2 anomaly peaks due to forest patches. However, our data show a localised, consistent CO_2 gas flux increase restricted to the scoria cone and its upper eastern flank, with random, transient (one to two data points) low-level flux increases (<20 g m^{-2} d^{-1}) elsewhere along the transect (Figure 4). Furthermore, the CO_2 flux profile is not symmetric about the scoria cone (segment B in Figure 4), which does not match the distribution expected if organic litter from the scrubland were the primary carbon dioxide source.

Statistical analysis of the anomalous Rangitoto CO_2 flux data (Figure 8) provides additional evidence against a biogenic origin. Cumulative probability analysis (Figure 8, following Chiodini et al. [1998] and Sinclair [1974, 1976]) indicates that anomalous flux measurements from all parts of the Rangitoto transect belong to a single population, as evidenced by their excellent fit ($R^2 = 0.99$) to a unique cumulative distribution function. This statistical uniformity, combined with the spatial distribution of CO_2 fluxes that do not correlate with surface vegetation patterns, suggests that the Rangitoto CO_2 anomaly originates from a deeper source rather than biogenic processes.

It is unlikely that the Rangitoto CO_2 gas emissions come from the cooling shallow (<300 m deep) basaltic body modelled under the Rangitoto scoria cone [Figure 7; Luthfian et al. 2023], which is thought to have solidified and can no longer degas CO_2 [cf. temporal evolution of CO_2 degassing from the similar composition and larger volume 1886 Tarawera magma; Hughes et al. 2019]. The bottom depth of this magmatic body is not well constrained by gravity and magnetic anomaly modelling [Luthfian et al. 2023] and might be in con-

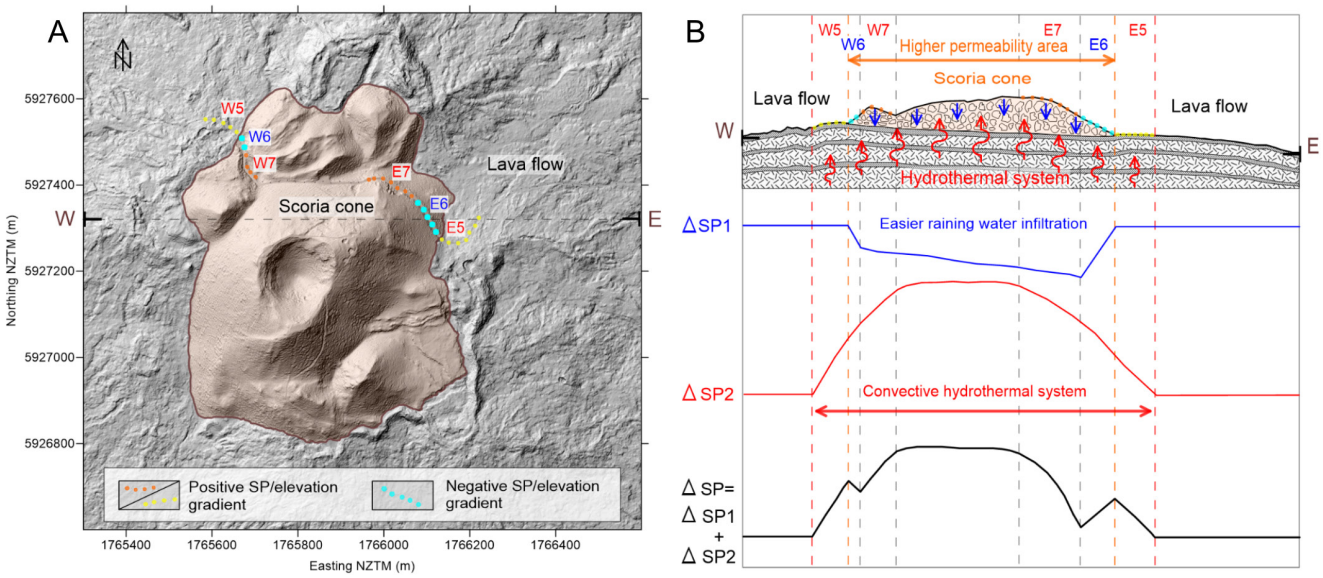

Figure 6: [A] SP measurements near the contact of Rangitoto scoria cones and lava fields where general positive and local negative SP/elevation gradient (C_e) are observed. Data points are coloured based on the order of their segments (5–7, see data label; same colour as in Figure 5), with the W/E prefix on the data label denoting the western or eastern side and the LiDAR base map from LINZ. Drill hole "RANG" is outside the map bounds, 200 m west of the 5 972 400 m Northing tick mark. [B] Top: A scheme of the interplay between meteoric fluid infiltration and hydrothermal fluid upflow under the Rangitoto scoria cones, with SP data points on the topography marked and labelled as in [A]. Subsurface geological sketch (not to scale) after Linnell et al. [2016]. The scoria cone's higher permeability (indicated by the orange arrow) promotes preferential rainwater infiltration. Bottom: SP signals from the rainwater infiltration (blue line) and hydrothermal fluid upflow (red line) add up to make the observed SP signal (black line).

tact with or very close to the Te Kuiti sediment at depths >320 m [e.g. the depth to Te Kuiti Group in drill hole #82630; Figure 1B; MBIE 2020]. However, considering the ~0.6 kya period elapsed since the last magmatic event, the temperature of hydrothermal fluids under Rangitoto circulating from a shallow intrusive body might be too cold [<400 °C; Valley 1986; Harris et al. 1997] to produce CO_2 from reactions with Te Kuiti group carbonate minerals. Plausible sources of these CO_2 emissions are deeper crustal intrusions, remobilisation of CO_2 from calcite veins within the basement [Melia et al. 2022], or mantle fluids seeping through a permeable pathway under Rangitoto (Figure 7), like Kamo and Ngāwhā springs near the Northland Volcanic Fields [Figure 1A; Giggenbach et al. 1993].

The deep origin of central Rangitoto CO_2 gas emission is also suggested by the relatively long wavelength of the anomaly (nearly 1 km; Figure 4) comparable to other active volcanoes (e.g. La Fossa of Vulcano; Revil et al. [2008]; Stromboli; Revil et al. [2011]). From structural geology vantage, we view that a network of fractures at depth can transport deep crustal CO_2 gas under Rangitoto to the surface. Potential fractures permeable for the rising CO_2 gas are near-surface joints, a continuation of westward-dipping Islington Bay Fault at depth, or extension of faults mapped south of Rangitoto volcano [e.g. Karaka Bay Fault and Bucklands Beach Fault; Figure 1B; Luthfian et al. 2023].

5.3 The Islington Bay and Motutapu faults

Near the Rangitoto-Motutapu bridge, a ~+60 mV offset separated the lower Rangitoto SP Block from the higher Motutapu SP Block (Figures 4 and 7). This step-like SP signal closely mimics the step-like gravity anomaly observed at the same location by Luthfian et al. [2023], indicating a common cause. Gravity anomaly modelling [Luthfian et al. 2023], supported by inference from topographic and remote sensing data [Kenny et al. 2012], suggests a buried Islington Bay Fault near the Rangitoto-Motutapu bridge (Figures 1, 2, 4, and 7). The step-like SP curve separating the Rangitoto and Motutapu blocks (Figures 4 and 7) may reflect the offsetting of near-surface aquifers or lithologies with different electrical properties by the Islington Bay Fault, similar to the one observed near the Eight-Mile Fault in Colorado, US [Revil et al. 2015]. The absence of deep-sourced CO_2 emission associated with the Islington Bay Fault (IBF in Figure 4) could be attributed to fault blockage from sealing, an underdeveloped damage zone, or a complex fault core and damage zone structure [Caine et al. 1996; Rowland and Sibson 2004]. Thus, the CO_2 may have been diverted/captured by other more permeable sub-Rangitoto pathways.

In contrast to the Islington Bay Fault, the Motutapu Fault ~800 m east of it is an exposed basement fault [Figures 1 and 2; Heron 2023]. The Motutapu Fault does not displace the outcropping Miocene Waitematā Group [Heron 2023]. The absence of SP and CO_2 gas flux signals associated with the Motutapu Fault (MF in Figure 4) suggests this structure might not be permeable.

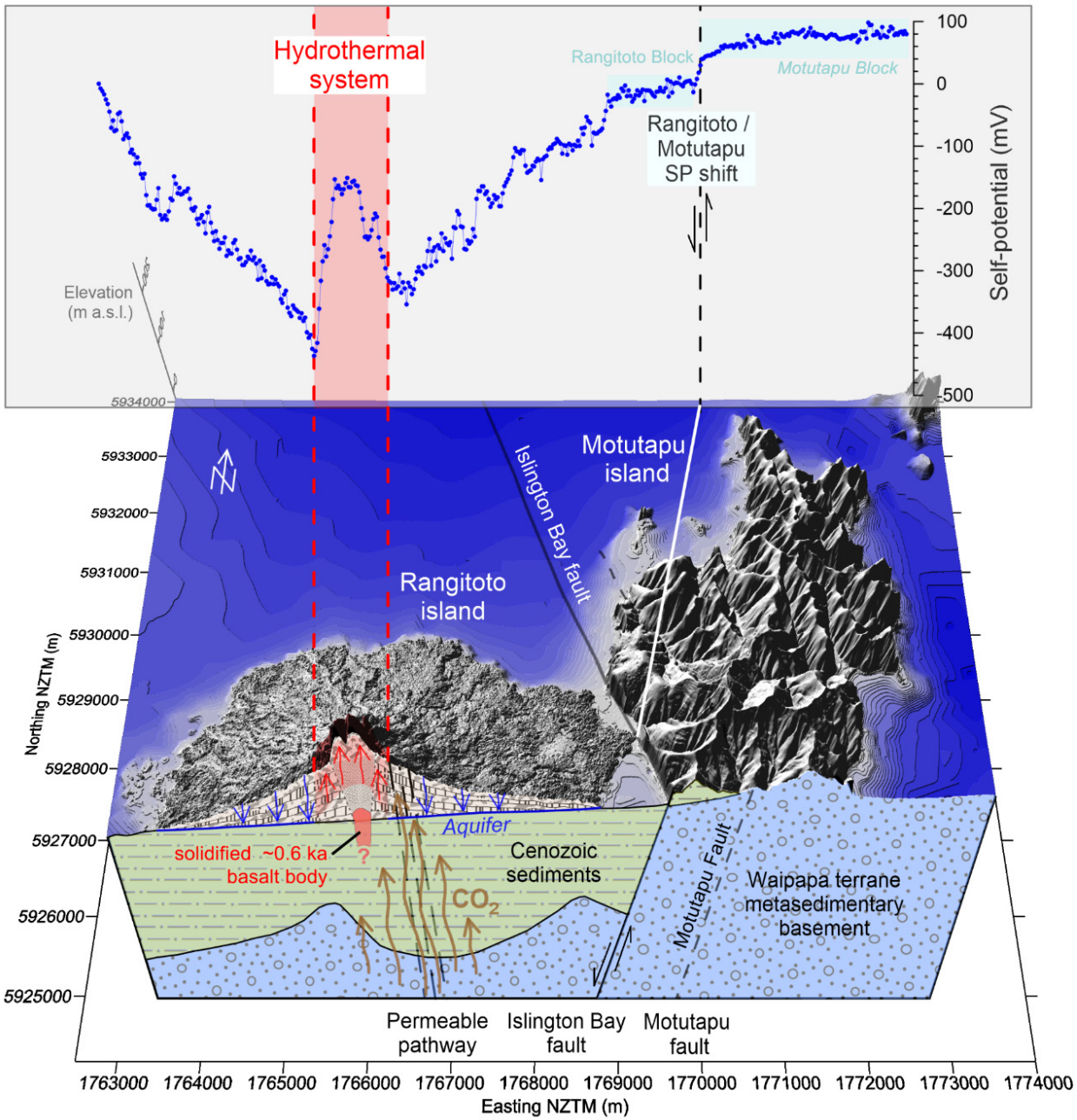

Figure 7: A Rangitoto–Motutapu hydrogeological system conceptual model (below) inferred from the SP-CO_2 gas flux data; only the SP electric potential curve is shown (above the model) for clarity. This model does not imply actual vertical depth. Cenozoic sediments (green) under Rangitoto comprise the Eocene Te Kuiti to recent sediments. We propose that the CO_2 gas comes from the basement or mantle sources and seeps through a permeable pathway under the Rangitoto edifice. Meanwhile, a heat source associated with the latest Rangitoto activity, e.g. cooling solidified magma body with a poorly constrained vertical extent (indicated by a "?"), warms the aquifer replenished by percolating meteoric water, creating an upward thermally driven upflow constituting the hydrothermal system revealed by the SP data. The Islington Bay Fault is associated with the Rangitoto–Motutapu SP shift, but no similar shift is associated with the Motutapu Fault.

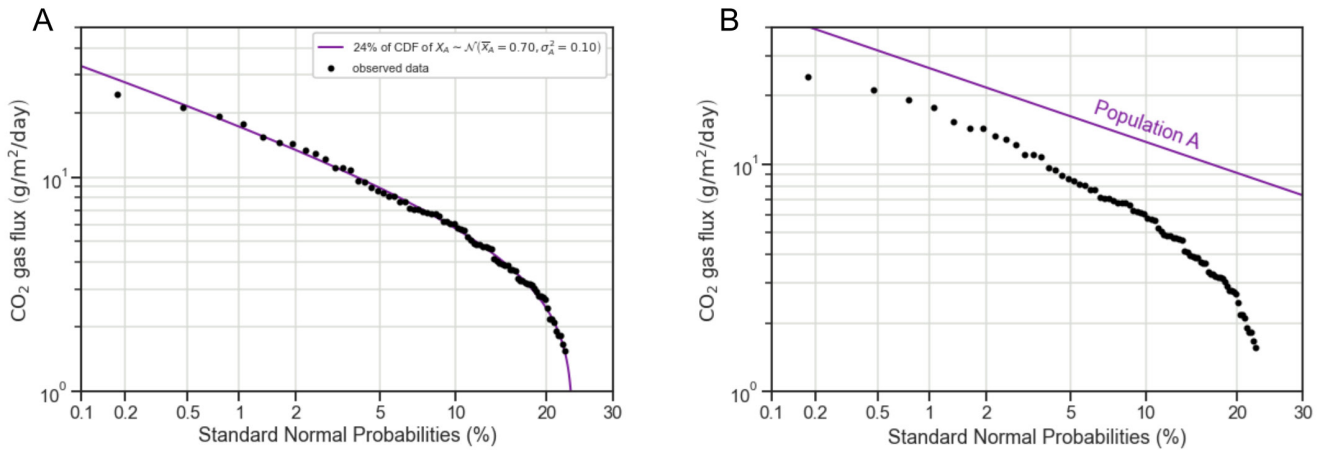

Figure 8: Figure 8: [A] Rangitoto anomalous gas flux's cumulative probability scatter fitted by 24 % of a normally distributed Population A with a mean of 0.70 g m^{-2} d^{-1} and a variance of 0.10 g m^{-2} d^{-1}. [B] The unscaled CDF of Population A is plotted against the Rangitoto anomalous gas flux's cumulative probability scatter (following Chiodini et al. [1998] and Sinclair [1974, 1976]).

6 Conclusions and Future Work

A combined SP-CO_2 gas flux study was carried out over the Rangitoto–Motutapu main road to explore signatures of hydrothermal activity associated with Rangitoto volcanism. The SP electric potential curve over Rangitoto indicates the presence of a hydrothermal system associated with the Rangitoto scoria cone. This hydrothermal system is likely heated by a source, e.g. a cooling basalt body, related to the latest Rangitoto volcanic activity at ~0.6 kya. The hydrothermal system is about 900 m in diameter. Inside this hydrothermal system, the corresponding positive SP/elevation gradient is disrupted by a short negative/elevation gradient associated with the lithological changes between the less permeable lava flow units and the very highly permeable Rangitoto scoria cone. Preferential water infiltration on the scoria cone is probably involved in this local SP decrease.

An elevated level of CO_2 gas flux is observed at the Rangitoto scoria cone, the upper part of the eastern flanks, and several small patches on the Rangitoto flanks. The Rangitoto sub-scoria cone basalt body has likely solidified and no longer degasses. At the same time, the sub-Rangitoto hydrothermal water temperature might be too cold to react with Te Kuiti carbonate rocks to produce CO_2. Therefore, we attribute these CO_2 emissions to deep crustal or mantle sources. This hypothesis is also supported by the ~620 m offset between SP and CO_2 peaks, suggesting a different origin for these two anomalies. A permeable pathway under Rangitoto might have captured and diverted rising CO_2 gas from other nearby basement faults, explaining the non-detection of CO_2 gas emissions over the Islington Bay and Motutapu faults.

This work illustrates the capability of SP and CO_2 gas flux explorations to qualitatively understand the hydrothermal and hydrological situation of a small-volume volcanic island. Nevertheless, as our CO_2 gas flux measurements were conducted following periods of rainfall when water-saturated near-surface materials can impede the upward migration of deep-sourced CO_2 gas [Viveiros et al. 2008], additional measurements during dry conditions would likely yield stronger deep-sourced CO_2 emission signals. Isotopic studies should also be done on Rangitoto diffuse CO_2 emission samples to validate our hypotheses regarding their origins. We also suggest that future electrical resistivity or induced polarisation tomography, which image near-surface resistivity or conductivity distribution under Rangitoto and Motutapu, will significantly improve the quantitative interpretation of SP and CO_2 gas flux data presented here.

Author Contributions

Alutsyah Luthfian: Investigation, Data Curation, Writing – Original Draft, Writing – Review & Editing. **Anthony Finizola** (Self-potential): Conceptualization, Methodology, Investigation, Software, Validation, Data Analysis, Field Equipment, Data Curation, Visualization, Acquisition, Supervision, Project Administration. **Agnes Mazot** (CO_2 gas flux): Methodology, Software, Investigation, Validation, Field Equipment, Data Analysis, Resources, Data Curation, Project Administration. **Ludmila Adam**: Writing–Review & Editing, Investigation, Data Curation, Project Administration, Funding and Data Acquisition. **Rachel Gusset**: Visualization, Data Curation (photography and video), Investigation. **Jennifer Eccles**: Writing – Review & Editing, Supervision, Permitting.

Acknowledgements

We thank Ngāi Tai ki Tāmaki iwi and the Department of Conservation for permitting us to do our mahi with their whānau and taonga in their sacred conservation area. We also appreciate their help with transportation during our Rangitoto and Motutapu fieldwork. Field work was funded by Ludmila Adam's University of Auckland RDA project. The Determining Volcanic Risk in Auckland (DEVORA) research programme sponsored Alutsyah Luthfian. INSU–CNRS and the Laboratoire GéoSciences Réunion–IPGP supported Anthony Finizola and Rachel Gusset. We thank an anonymous reviewer and Marceau Gresse for their thoughtful reviews and

suggestions that improved the logical coherence and scientific quality of the ideas proposed in this work.

Data Availability

Data used in this study is available as a supplementary material and in this GitHub URL: https://github.com/aluthfian/Rangitoto_SP_gasFlux.

Auckland 1 m resolution LiDAR DEM is available from the official Land Information New Zealand (LINZ) website: https://data.linz.govt.nz/layer/106410-auckland-north-lidar-1m-dem-2016-2018/.

Copyright notice

References

Aggarwal, J. K., D. Sheppard, K. Mezger, and E. Pernicka (2003). "Precise and accurate determination of boron isotope ratios by multiple collector ICP–MS: origin of boron in the Ngawha geothermal system, New Zealand". *Chemical Geology* 199(3–4), pages 331–342. DOI: 10.1016/s0009-2541(03)00127-x.

Aizawa, K., R. Yoshimura, N. Oshiman, K. Yamazaki, T. Uto, Y. Ogawa, S. Tank, W. Kanda, S. Sakanaka, and Y. Furukawa (2005). "Hydrothermal system beneath Mt. Fuji volcano inferred from magnetotellurics and electric self-potential". *Earth and Planetary Science Letters* 235(1–2), pages 343–355. DOI: 10.1016/j.epsl.2005.03.023.

Aizawa, K. (2008). "Classification of self-potential anomalies on volcanoes and possible interpretations for their subsurface structure". *Journal of Volcanology and Geothermal Research* 175(3), pages 253–268. DOI: 10.1016/j.jvolgeores.2008.03.011.

Aizawa, K., Y. Ogawa, and T. Ishido (2009). "Groundwater flow and hydrothermal systems within volcanic edifices: Delineation by electric self-potential and magnetotellurics". *Journal of Geophysical Research: Solid Earth* 114(B1). DOI: 10.1029/2008jb005910.

Aizawa, K., M. Uyeshima, and K. Nogami (2008). "Zeta potential estimation of volcanic rocks on 11 island arc-type volcanoes in Japan: Implication for the generation of local self-potential anomalies". *Journal of Geophysical Research: Solid Earth* 113(B2). DOI: 10.1029/2007jb005058.

Allington, M. L., A. Nilsson, M. J. Hill, N. Suttie, D. Daniil, I. Hjorth, L. Aulin, P. C. Augustinus, and P. Shane (2023). "Constraining the eruption history of Rangitoto volcano, New Zealand, using palaeomagnetic data". *Quaternary Geochronology* 78, page 101459. DOI: 10.1016/j.quageo.2023.101459.

Beanland, S. and J. Haines (1998). "The kinematics of active deformation in the North Island, New Zealand, determined from geological strain rates". *New Zealand Journal of Geology and Geophysics* 41(4), pages 311–323. DOI: 10.1080/00288306.1998.9514813.

Bebbington, M. S. (2015). "Spatio-volumetric hazard estimation in the Auckland volcanic field". *Bulletin of Volcanology* 77(5). DOI: 10.1007/s00445-015-0921-3.

Bennati, L., A. Finizola, J. A. Walker, D. L. Lopez, I. C. Higuera-Diaz, C. Schütze, F. Barahona, R. Cartagena, V. Conde, R. Funes, and C. Rios (2011). "Fluid circulation in a complex volcano-tectonic setting, inferred from self-potential and soil CO_2 flux surveys: The Santa María–Cerro Quemado–Zunil volcanoes and Xela caldera (Northwestern Guatemala)". *Journal of Volcanology and Geothermal Research* 199(3–4), pages 216–229. DOI: 10.1016/j.jvolgeores.2010.11.008.

Bolós, X., A. Delgado-Torres, G. Cifuentes, J. L. Macías, M. Boijseauneau-López, C. Tinoco, and D. Salguero (2020). "Internal structure and hydrothermal fluid circulation of Parícutin Volcano, Mexico: Insights gained from near-surface geophysics". *Geophysical Research Letters* 47(16). DOI: 10.1029/2020gl089270.

Bond, C. E., Y. Kremer, G. Johnson, N. Hicks, R. Lister, D. G. Jones, R. S. Haszeldine, I. Saunders, S. M. Gilfillan, Z. K. Shipton, and J. Pearce (2017). "The physical characteristics of a CO_2 seeping fault: The implications of fracture permeability for carbon capture and storage integrity". *International Journal of Greenhouse Gas Control* 61, pages 49–60. DOI: 10.1016/j.ijggc.2017.01.015.

Briggs, R. M., T. Okada, T. Itaya, H. Shibuya, and I. E. M. Smith (1994). "K–Ar ages, paleomagnetism, and geochemistry of the South Auckland volcanic field, North Island, New Zealand". *New Zealand Journal of Geology and Geophysics* 37(2), pages 143–153. DOI: 10.1080/00288306.1994.9514609.

Browne, P. R. L. and J. V. Lawless (2001). "Characteristics of hydrothermal eruptions, with examples from New Zealand and elsewhere". *Earth-Science Reviews* 52(4), pages 299–331. DOI: 10.1016/s0012-8252(00)00030-1.

Byrdina, S., J. Vandemeulebrouck, C. Cardellini, A. Legaz, C. Camerlynck, G. Chiodini, T. Lebourg, M. Gresse, P. Bascou, G. Motos, A. Carrier, and S. Caliro (2014). "Relations between electrical resistivity, carbon dioxide flux, and self-potential in the shallow hydrothermal system of Solfatara (Phlegrean Fields, Italy)". *Journal of Volcanology and Geothermal Research* 283, pages 172–182. DOI: 10.1016/j.jvolgeores.2014.07.010.

Caine, J. S., J. P. Evans, and C. B. Forster (1996). "Fault zone architecture and permeability structure". *Geology* 24(11), page 1025. DOI: 10.1130/0091-7613(1996)024<1025:fzaaps>2.3.co;2.

Cathles, L. M., A. H. J. Erendi, and T. Barrie (1997). "How long can a hydrothermal system be sustained by a single intrusive event?" *Economic Geology* 92(7–8), pages 766–771. DOI: 10.2113/gsecongeo.92.7-8.766.

Chiodini, G., R. Cioni, M. Guidi, B. Raco, and L. Marini (1998). "Soil CO_2 flux measurements in volcanic and geothermal areas". *Applied Geochemistry* 13(5), pages 543–552. DOI: 10.1016/s0883-2927(97)00076-0.

Connor, C. B., P. C. Lichtner, F. M. Conway, B. E. Hill, A. A. Ovsyannikov, I. Federchenko, Y. Doubik, V. N. Shapar, and Y. A. Taran (1997). "Cooling of an igneous dike 20 yr after intrusion". *Geology* 25(8), page 711. DOI: 10.1130/0091-7613(1997)025<0711:coaidy>2.3.co;2.

Davy, B. (2008). "Marine seismic reflection profiles from the Waitemata–Whangaparoa region, Auckland". *New Zealand Journal of Geology and Geophysics* 51(3), pages 161–173. DOI: 10.1080/00288300809509857.

DeMets, C., R. G. Gordon, D. F. Argus, and S. Stein (1994). "Effect of recent revisions to the geomagnetic reversal time scale on estimates of current plate motions". *Geophysical Research Letters* 21(20), pages 2191–2194. DOI: 10.1029/94gl02118.

Driesner, T. and S. Geiger (2007). "Numerical simulation of multiphase fluid flow in hydrothermal systems". *Reviews in Mineralogy and Geochemistry* 65(1), pages 187–212. DOI: 10.2138/rmg.2007.65.6.

Eccles, J., J. Cassidy, C. Locke, and K. Spörli (2005). "Aeromagnetic imaging of the Dun Mountain Ophiolite Belt in northern New Zealand: insight into the fine structure of a major SW Pacific terrane suture". *Journal of the Geological Society* 162(4), pages 723–735. DOI: 10.1144/0016-764904-060.

Edbrooke, S. W. (2001). *Geology of the Auckland area (1:250,000 geological map 3)*. URL: https://shop.gns.cri.nz/mqm3/. New Zealand: Institute of Geological & Nuclear Sciences Limited. 74 pages.

Edbrooke, S. W., E. M. Crouch, H. E. G. Morgans, and R. Sykes (1998). "Late Eocene–Oligocene Te Kuiti Group at Mount Roskill, Auckland, New Zealand". *New Zealand Journal of Geology and Geophysics* 41(1), pages 85–93. DOI: 10.1080/00288306.1998.9514792.

Ensing, J. X., K. van Wijk, and K. B. Spörli (2022). "A 3D crustal shear speed model of the Auckland volcanic field, New Zealand, from multi-component ambient noise tomography". *Tectonophysics* 845, page 229627. DOI: 10.1016/j.tecto.2022.229627.

Finizola, A., A. Revil, E. Rizzo, S. Piscitelli, T. Ricci, J. Morin, B. Angeletti, L. Mocochain, and F. Sortino (2006). "Hydrogeological insights at Stromboli volcano (Italy) from geoelectrical, temperature, and CO_2 soil degassing investigations". *Geophysical Research Letters* 33(17). DOI: 10.1029/2006gl026842.

Finizola, A., T. Ricci, R. Deiana, S. B. Cabusson, M. Rossi, N. Praticelli, A. Giocoli, G. Romano, E. Delcher, B. Suski, A. Revil, P. Menny, F. Di Gangi, J. Letort, A. Peltier, V. Villasante-Marcos, G. Douillet, G. Avard, and M. Lelli (2010). "Adventive hydrothermal circulation on Stromboli volcano (Aeolian Islands, Italy) revealed by geophysical and geochemical approaches: Implications for general fluid flow models on volcanoes". *Journal of Volcanology and Geothermal Research* 196(1–2), pages 111–119. DOI: 10.1016/j.jvolgeores.2010.07.022.

Finizola, A., J.-F. Lénat, O. Macedo, D. Ramos, J.-C. Thouret, and F. Sortino (2004). "Fluid circulation and structural discontinuities inside Misti volcano (Peru) inferred from self-potential measurements". *Journal of Volcanology and Geothermal Research* 135(4), pages 343–360. DOI: 10.1016/j.jvolgeores.2004.03.009.

Finizola, A., F. Sortino, J.-F. Lénat, M. Aubert, M. Ripepe, and M. Valenza (2003). "The summit hydrothermal system of Stromboli. New insights from self-potential, temperature, CO_2 and fumarolic fluid measurements, with structural and monitoring implications". *Bulletin of Volcanology* 65(7), pages 486–504. DOI: 10.1007/s00445-003-0276-z.

Finizola, A., F. Sortino, J.-F. Lénat, and M. Valenza (2002). "Fluid circulation at Stromboli volcano (Aeolian Islands, Italy) from self-potential and CO_2 surveys". *Journal of Volcanology and Geothermal Research* 116(1–2), pages 1–18. DOI: 10.1016/s0377-0273(01)00327-4.

Gaskin, C. (1990). *Sunde Site, Motutapu, after the eruption of Rangitoto*. https://www.aucklandmuseum.com/collection/object/996907. [Watercolour on card]. Auckland Museum, Auckland, New Zealand.

Giba, M., A. Nicol, and J. J. Walsh (2010). "Evolution of faulting and volcanism in a back-arc basin and its implications for subduction processes". *Tectonics* 29(4). DOI: 10.1029/2009tc002634.

Giggenbach, W. F., Y. Sano, and H. Wakita (1993). "Isotopic composition of helium, and CO_2 and CH_4 contents in gases produced along the New Zealand part of a convergent plate boundary". *Geochimica et Cosmochimica Acta* 57(14), pages 3427–3455. DOI: 10.1016/0016-7037(93)90549-c.

GNS Science (1970). *GeoNet Aotearoa New Zealand Earthquake Catalogue*. DOI: 10.21420/0S8P-TZ38.

Granieri, D., R. Avino, and G. Chiodini (2010). "Carbon dioxide diffuse emission from the soil: ten years of observations at Vesuvio and Campi Flegrei (Pozzuoli), and linkages with volcanic activity". *Bulletin of Volcanology* 72(1), pages 103–118. DOI: 10.1007/s00445-009-0304-8.

Gresse, M., M. Uyeshima, T. Koyama, H. Hase, K. Aizawa, Y. Yamaya, Y. Morita, D. Weller, T. Rung-Arunwan, T. Kaneko, Y. Sasai, J. Zlotnicki, T. Ishido, H. Ueda, and M. Hata (2021). "Hydrothermal and magmatic system of a volcanic island inferred from magnetotellurics, seismicity, self-potential, and thermal image: An example of Miyakejima (Japan)". *Journal of Geophysical Research: Solid Earth* 126(6). DOI: 10.1029/2021jb022034.

Gresse, M., J. Vandemeulebrouck, S. Byrdina, G. Chiodini, A. Revil, T. C. Johnson, T. Ricci, G. Vilardo, A. Mangiacapra, T. Lebourg, J. Grangeon, P. Bascou, and L. Metral (2017). "Three-dimensional electrical resistivity tomography of the Solfatara Crater (Italy): Implication for the multiphase flow structure of the shallow hydrothermal system". *Journal of Geophysical Research: Solid Earth* 122(11), pages 8749–8768. DOI: 10.1002/2017jb014389.

Hanson, M. C., C. Oze, and T. W. Horton (2014). "Identifying blind geothermal systems with soil CO_2 surveys". *Applied Geochemistry* 50, pages 106–114. DOI: 10.1016/j.apgeochem.2014.08.009.

Harris, C., W. Stock, and J. Lanham (1997). "Stable isotope constraints on the origin of CO_2 gas exhalations at Bongwan, Natal". *South African Journal of Geology* 100(3), pages 261–266.

Hashimoto, S. and H. Komatsu (2006). "Relationships between soil CO_2 concentration and CO_2 production, temperature, water content, and gas diffusivity: implications for field studies through sensitivity analyses". *Journal of Forest Research* 11(1), pages 41–50. DOI: 10.1007/s10310-005-0185-4.

Hayward, B. W. (2022). "Origins of baked and unbaked sediment packages within Rangitoto lava flows". *Geocene: Auckland GeoClub Magazine* 30, pages 2–5.

Hayward, B. W. and A. Jamieson (2019). *Volcanoes of Auckland: A Field Guide*. Auckland University Press. 344 pages. ISBN: 9781869409012.

Hayward, B. W., J. L. Hopkins, M. Morley, and J. A. Kenny (2022). "Microfossil evidence for a possible maar crater and tuff ring beneath Rangitoto Volcano, Auckland, New Zealand". *New Zealand Journal of Geology and Geophysics* 67(1), pages 121–137. DOI: 10.1080/00288306.2022.2120505.

Heron, D. W. (2023). *Geological Map of New Zealand 1:250 000*. 4th edition. Lower Hutt, New Zealand: GNS Science. DOI: 10.21420/5XTJ-5718. [Digital data].

Hobson, B. (1907). "An excursion to the volcanoes of Nevado de Toluca and Jorullo in Mexico". *Geological Magazine* 4(1), pages 5–13. DOI: 10.1017/s0016756800128791.

Hopkins, J. L., E. R. Smid, J. D. Eccles, J. L. Hayes, B. W. Hayward, L. E. McGee, K. van Wijk, T. M. Wilson, S. J. Cronin, G. S. Leonard, J. M. Lindsay, K. Németh, and I. E. M. Smith (2020). "Auckland Volcanic Field magmatism, volcanism, and hazard: a review". *New Zealand Journal of Geology and Geophysics* 64(2–3), pages 213–234. DOI: 10.1080/00288306.2020.1736102.

Hu, R., K. Kusa, and R. Hatano (2001). "Soil respiration and methane flux in adjacent forest, grassland, and cornfield soils in Hokkaido, Japan". *Soil Science and Plant Nutrition* 47(3), pages 621–627. DOI: 10.1080/00380768.2001.10408425.

Huang, Y., C. Hawkesworth, I. Smith, P. van Calsteren, and P. Black (2000). "Geochemistry of late Cenozoic basaltic volcanism in Northland and Coromandel, New Zealand: implications for mantle enrichment processes". *Chemical Geology* 164(3–4), pages 219–238. DOI: 10.1016/s0009-2541(99)00145-x.

Huang, Y., C. Hawkesworth, P. van Calsteren, I. Smith, and P. Black (1997). "Melt generation models for the Auckland volcanic field, New Zealand: constraints from U–Th isotopes". *Earth and Planetary Science Letters* 149(1–4), pages 67–84. DOI: 10.1016/s0012-821x(97)00064-2.

Hughes, E. C., A. Mazot, G. Kilgour, C. Asher, M. Michelini, K. Britten, L. Chardot, Y. Feisel, and C. Werner (2019). "Understanding degassing pathways along the 1886 Tarawera (New Zealand) volcanic fissure by combining soil and lake CO_2 fluxes". *Frontiers in Earth Science* 7. DOI: 10.3389/feart.2019.00264.

Irwin, M. (2009). *Synthesis of existing structural data for the Auckland Volcanic Field*. Technical report. DOI: 10.17608/K6.AUCKLAND.10250795.V1.

Ishido, T. (2004). "Electrokinetic mechanism for the "W"-shaped self-potential profile on volcanoes". *Geophysical Research Letters* 31(15). DOI: 10.1029/2004gl020409.

Ishido, T. and H. Mizutani (1981). "Experimental and theoretical basis of electrokinetic phenomena in rock-water systems and its applications to geophysics". *Journal of Geophysical Research: Solid Earth* 86(B3), pages 1763–1775. DOI: 10.1029/jb086ib03p01763.

Jácome-Paz, M. P., H. Delgado-Granados, X. Pérez-Campos, R. Espinasa-Pereña, and R. Campion (2022). "Diffuse degassing baseline in Parícutin volcano and Michoacán–Guanajuato monogenetic volcanic field, México". *Journal of Volcanology and Geothermal Research* 425, page 107534. DOI: 10.1016/j.jvolgeores.2022.107534.

Jakobsson, S. P. and J. G. Moore (1986). "Hydrothermal minerals and alteration rates at Surtsey volcano, Iceland". *Geological Society of America Bulletin* 97(5), page 648. DOI: 10.1130/0016-7606(1986)97<648:hmaara>2.0.co;2.

Jennings, K. J., J. D. Muirhead, K. B. Spörli, and L. J. Strachan (2023). "Towards a tectonic framework for normal faults in Waitematā Group rocks, North Island, Aotearoa–New Zealand". *New Zealand Journal of Geology and Geophysics* 68(1), pages 80–94. DOI: 10.1080/00288306.2023.2268010.

Julian, A. (1992). "The vegetation pattern of Rangitoto". Doctoral Thesis.

Kear, D. (1964). "Volcanic alignments North and West of New Zealand's Central Volcanic Region". *New Zealand Journal of Geology and Geophysics* 7(1), pages 24–44. DOI: 10.1080/00288306.1964.10420155.

Kenny, J. A., J. M. Lindsay, and T. M. Howe (2012). "Post-Miocene faults in Auckland: insights from borehole and topographic analysis". *New Zealand Journal of Geology and Geophysics* 55(4), pages 323–343. DOI: 10.1080/00288306.2012.706618.

Kereszturi, G. and K. Németh (2016). "Sedimentology, eruptive mechanism and facies architecture of basaltic scoria cones from the Auckland Volcanic Field (New Zealand)". *Journal of Volcanology and Geothermal Research* 324, pages 41–56. DOI: 10.1016/j.jvolgeores.2016.05.012.

Kereszturi, G., K. Németh, S. J. Cronin, J. Agustín-Flores, I. E. Smith, and J. Lindsay (2013). "A model for calculating eruptive volumes for monogenetic volcanoes—Implication for the Quaternary Auckland Volcanic Field, New Zealand". *Journal of Volcanology and Geothermal Research* 266, pages 16–33. DOI: 10.1016/j.jvolgeores.2013.09.003.

Kermode, L. O. (1992). *Geology of the Auckland urban area (1:50,000 geological map 2)*. URL: https://shop.gns.cri.nz/gm2-pdf/. New Zealand: Institute of Geological & Nuclear Sciences Limited. 63 pages.

Kühn, M. and H. Stöfen (2005). "A reactive flow model of the geothermal reservoir Waiwera, New Zealand". *Hydrogeology Journal* 13(4), pages 606–626. DOI: 10.1007/s10040-004-0377-6.

Laiolo, M., M. Ranaldi, L. Tarchini, M. L. Carapezza, D. Coppola, T. Ricci, and C. Cigolini (2016). "The effects of environmental parameters on diffuse degassing at Stromboli volcano: Insights from joint monitoring of soil CO_2 flux and

radon activity". *Journal of Volcanology and Geothermal Research* 315, pages 65–78. DOI: 10.1016/j.jvolgeores.2016.02.004.

Land Information New Zealand (2018). *Auckland North LiDAR 1m DEM (2016–2018)*. https://data.linz.govt.nz/layer/106410-auckland-north-lidar-1m-dem-2016-2018/.

Le Corvec, N., K. B. Spörli, J. Rowland, and J. Lindsay (2013). "Spatial distribution and alignments of volcanic centers: Clues to the formation of monogenetic volcanic fields". *Earth-Science Reviews* 124, pages 96–114. DOI: 10.1016/j.earscirev.2013.05.005.

Lénat, J.-F. (2007). "Retrieving self-potential anomalies in a complex volcanic environment: an SP/elevation gradient approach". *Near Surface Geophysics* 5(3), pages 161–170. DOI: 10.3997/1873-0604.2006028.

Leonard, G. S., A. T. Calvert, J. L. Hopkins, C. J. Wilson, E. R. Smid, J. M. Lindsay, and D. E. Champion (2017). "High-precision 40 Ar/39 Ar dating of Quaternary basalts from Auckland Volcanic Field, New Zealand, with implications for eruption rates and paleomagnetic correlations". *Journal of Volcanology and Geothermal Research* 343, pages 60–74. DOI: 10.1016/j.jvolgeores.2017.05.033.

Lewicki, J. L., W. C. Evans, G. E. Hilley, M. L. Sorey, J. D. Rogie, and S. L. Brantley (2003). "Shallow soil CO_2 flow along the San Andreas and Calaveras Faults, California". *Journal of Geophysical Research: Solid Earth* 108(B4). DOI: 10.1029/2002jb002141.

Linde, N., A. Revil, A. Bolève, C. Dagès, J. Castermant, B. Suski, and M. Voltz (2007). "Estimation of the water table throughout a catchment using self-potential and piezometric data in a Bayesian framework". *Journal of Hydrology* 334(1–2), pages 88–98. DOI: 10.1016/j.jhydrol.2006.09.027.

Linnell, T., P. Shane, I. Smith, P. Augustinus, S. Cronin, J. Lindsay, and R. Maas (2016). "Long-lived shield volcanism within a monogenetic basaltic field: The conundrum of Rangitoto volcano, New Zealand". *Geological Society of America Bulletin* 128(7–8), pages 1160–1172. DOI: 10.1130/b31392.1.

Lowe, D., R. Newnham, and J. McCraw (2002). "Volcanism and early Maori society in New Zealand". *Natural Disasters and Cultural Change*. Edited by J. Grattan and R. Torrence. 1st Edition, pages 126–161. ISBN: 9780203165102. DOI: 10.4324/9780203165102.

Lube, G., E. C. Breard, S. J. Cronin, J. N. Procter, M. Brenna, A. Moebis, N. Pardo, R. B. Stewart, A. Jolly, and N. Fournier (2014). "Dynamics of surges generated by hydrothermal blasts during the 6 August 2012 Te Maari eruption, Mt. Tongariro, New Zealand". *Journal of Volcanology and Geothermal Research* 286, pages 348–366. DOI: 10.1016/j.jvolgeores.2014.05.010.

Luthfian, A., J. D. Eccles, and C. A. Miller (2023). "Gravity and magnetic models at Rangitoto Volcano, Auckland Volcanic Field, New Zealand: Implications for basement control on magma ascent". *Journal of Volcanology and Geothermal Research* 439, page 107824. DOI: 10.1016/j.jvolgeores.2023.107824.

MacAllister, D. J., M. D. Jackson, A. P. Butler, and J. Vinogradov (2016). "Tidal influence on self-potential measurements". *Journal of Geophysical Research: Solid Earth* 121(12), pages 8432–8452. DOI: 10.1002/2016jb013376.

Mackay, K., E. Mackay, H. Neil, J. Mitchell, and S. Bardsley (2012). *Hauraki Gulf [Bathymetric grid data]*. URL: https://dc.niwa.co.nz/niwa_dc/srv/api/records/77ea2419-c634-0bf8-c829-d7607036ec96. National Institute of Water & Atmospheric Research.

Mayer, W. (1968). "The stratigraphy and structure of the Waipapa Group on the islands of Motutapu, Rakino, and the Noisies Group near Auckland, New Zealand". *Transactions of the Royal Society of New Zealand: Geology* 5(9), pages 215–233.

Maza, S. N., G. Collo, D. Morata, C. Lizana, E. Camus, M. Taussi, A. Renzulli, M. Mattioli, B. Godoy, B. Alvear, M. Pizarro, C. Ramírez, and G. Rivera (2018). "Clay mineral associations in the clay cap from the Cerro Pabellón blind geothermal system, Andean Cordillera, Northern Chile". *Clay Minerals* 53(2), pages 117–141. DOI: 10.1180/clm.2018.9.

Mazot, A., E. R. Smid, L. Schwendenmann, H. Delgado-Granados, and J. Lindsay (2013). "Soil CO_2 flux baseline in an urban monogenetic volcanic field: the Auckland Volcanic Field, New Zealand". *Bulletin of Volcanology* 75(11). DOI: 10.1007/s00445-013-0757-7.

MBIE (2020). *New Zealand Geotechnical Database*. https://www.nzgd.org.nz.

McGee, L. E., I. E. M. Smith, M.-A. Millet, H. K. Handley, and J. M. Lindsay (2013). "Asthenospheric control of melting processes in a monogenetic basaltic system: a case study of the Auckland Volcanic Field, New Zealand". *Journal of Petrology* 54(10), pages 2125–2153. DOI: 10.1093/petrology/egt043.

McGee, L. E. and I. E. Smith (2016). "Interpreting chemical compositions of small scale basaltic systems: A review". *Journal of Volcanology and Geothermal Research* 325, pages 45–60. DOI: 10.1016/j.jvolgeores.2016.06.007.

Melia, A., D. R. Faulkner, and D. D. McNamara (2022). "Physical property characterization of the Waipapa greywacke: an important geothermal reservoir basement rock in New Zealand". *Geothermal Energy* 10(1). DOI: 10.1186/s40517-022-00218-2.

Needham, A. J., J. M. Lindsay, I. E. M. Smith, P. Augustinus, and P. A. Shane (2011). "Sequential eruption of alkaline and sub-alkaline magmas from a small monogenetic volcano in the Auckland Volcanic Field, New Zealand". *Journal of Volcanology and Geothermal Research* 201(1–4), pages 126–142. DOI: 10.1016/j.jvolgeores.2010.07.017.

Nichol, R. (1992). "The eruption history of Rangitoto: reappraisal of a small New Zealand myth". *Journal of the Royal Society of New Zealand* 22(3), pages 159–180. DOI: 10.1080/03036758.1992.10426554.

Norton, D. L. (1984). "Theory of hydrothermal systems". *Annual Review of Earth and Planetary Sciences* 12(1), pages 155–177. DOI: 10.1146/annurev.ea.12.050184.001103.

Norton, D. L. and J. E. Knight (1977). "Transport phenomena in hydrothermal systems; cooling plutons". *American Journal of Science* 277(8), pages 937–981. DOI: 10.2475/ajs.277.8.937.

Onizawa, S., N. Matsushima, T. Ishido, H. Hase, S. Takakura, and Y. Nishi (2009). "Self-potential distribution on active volcano controlled by three-dimensional resistivity structure in Izu-Oshima, Japan". *Geophysical Journal International* 178(2), pages 1164–1181. DOI: 10.1111/j.1365-246x.2009.04203.x.

Parson, L. M. and I. C. Wright (1996). "The Lau–Havre–Taupo back-arc basin: A southward-propagating, multi-stage evolution from rifting to spreading". *Tectonophysics* 263(1–4), pages 1–22. DOI: 10.1016/s0040-1951(96)00029-7.

Poblete Piedrabuena, M. Á., S. Beato Bergua, and J. L. Marino Alfonso (2016). "Landforms in the Campo de Calatrava Volcanic Field (Ciudad Real, Central Spain)". *Journal of Maps* 12(sup1), pages 271–279. DOI: 10.1080/17445647.2016.1195302.

Price, R. C., R. B. Stewart, J. D. Woodhead, and I. E. M. Smith (1999). "Petrogenesis of high-K arc magmas: Evidence from Egmont Volcano, North Island, New Zealand". *Journal of Petrology* 40(1), pages 167–197. DOI: 10.1093/petroj/40.1.167.

Raich, J. W. and A. Tüfekçioğlu (2000). "Vegetation and soil respiration: Correlations and controls". *Biogeochemistry* 48(1), pages 71–90. DOI: 10.1023/a:1006112000616.

Revil, A., Y. Qi, A. Ghorbani, A. Coperey, A. S. Ahmed, A. Finizola, and T. Ricci (2019). "Induced polarization of volcanic rocks. 3. Imaging clay cap properties in geothermal fields". *Geophysical Journal International* 218(2), pages 1398–1427. DOI: 10.1093/gji/ggz207.

Revil, A., S. Cuttler, M. Karaoulis, J. Zhou, B. Raynolds, and M. Batzle (2015). "The plumbing system of the Pagosa thermal springs, Colorado: Application of geologically constrained geophysical inversion and data fusion". *Journal of Volcanology and Geothermal Research* 299, pages 1–18. DOI: 10.1016/j.jvolgeores.2015.04.005.

Revil, A., A. Finizola, and M. Gresse (2023). "Self-potential as a tool to assess groundwater flow in hydrothermal systems: A review". *Journal of Volcanology and Geothermal Research* 437, page 107788. DOI: 10.1016/j.jvolgeores.2023.107788.

Revil, A., A. Finizola, S. Piscitelli, E. Rizzo, T. Ricci, A. Crespy, B. Angeletti, M. Balasco, S. Barde Cabusson, L. Bennati, A. Bolève, S. Byrdina, N. Carzaniga, F. Di Gangi, J. Morin, A. Perrone, M. Rossi, E. Roulleau, and B. Suski (2008). "Inner structure of La Fossa di Vulcano (Vulcano Island, southern Tyrrhenian Sea, Italy) revealed by high-resolution electric resistivity tomography coupled with self-potential, temperature, and CO_2 diffuse degassing measurements". *Journal of Geophysical Research: Solid Earth* 113(B7). DOI: 10.1029/2007jb005394.

Revil, A., A. Finizola, T. Ricci, E. Delcher, A. Peltier, S. Barde-Cabusson, G. Avard, T. Bailly, L. Bennati, S. Byrdina, J. Colonge, F. Di Gangi, G. Douillet, M. Lupi, J. Letort, and E. Tsang Hin Sun (2011). "Hydrogeology of Stromboli volcano, Aeolian Islands (Italy) from the interpretation of resistivity tomograms, self-potential, soil temperature and soil CO_2 concentration measurements". *Geophysical Journal International* 186(3), pages 1078–1094. DOI: 10.1111/j.1365-246x.2011.05112.x.

Revil, A., A. Finizola, F. Sortino, and M. Ripepe (2004). "Geophysical investigations at Stromboli volcano, Italy: implications for ground water flow and paroxysmal activity". *Geophysical Journal International* 157(1), pages 426–440. DOI: 10.1111/j.1365-246x.2004.02181.x.

Revil, A., Y. Qi, S. Barde-Cabusson, and M. Gresse (2021). "Induced polarization of the 1630-monogenetic dome, Furnas volcano, São Miguel Island, Azores archipelago". *Journal of Volcanology and Geothermal Research* 420, page 107410. DOI: 10.1016/j.jvolgeores.2021.107410.

Revil, A. and A. Jardani (2013). *The self-potential method: Theory and applications in environmental geosciences*. Cambridge University Press. ISBN: 9781107019270. DOI: 10.1017/cbo9781139094252.

Richards, K., A. Revil, A. Jardani, F. Henderson, M. Batzle, and A. Haas (2010). "Pattern of shallow ground water flow at Mount Princeton Hot Springs, Colorado, using geoelectrical methods". *Journal of Volcanology and Geothermal Research* 198(1–2), pages 217–232. DOI: 10.1016/j.jvolgeores.2010.09.001.

Riggs, N. R. and W. A. Duffield (2008). "Record of complex scoria cone eruptive activity at Red Mountain, Arizona, USA, and implications for monogenetic mafic volcanoes". *Journal of Volcanology and Geothermal Research* 178(4), pages 763–776. DOI: 10.1016/j.jvolgeores.2008.09.004.

Rowland, J. V. and R. H. Sibson (2004). "Structural controls on hydrothermal flow in a segmented rift system, Taupo Volcanic Zone, New Zealand". *Geofluids* 4(4), pages 259–283. DOI: 10.1111/j.1468-8123.2004.00091.x.

Saar, M. O. and M. Manga (1999). "Permeability-porosity relationship in vesicular basalts". *Geophysical Research Letters* 26(1), pages 111–114. DOI: 10.1029/1998gl900256.

Shane, P., M. Gehrels, A. Zawalna-Geer, P. Augustinus, J. Lindsay, and I. Chaillou (2013). "Longevity of a small shield volcano revealed by crypto-tephra studies (Rangitoto volcano, New Zealand): Change in eruptive behavior of a basaltic field". *Journal of Volcanology and Geothermal Research* 257, pages 174–183. DOI: 10.1016/j.jvolgeores.2013.03.026.

Sinclair, A. J. (1976). *Applications of probability graphs in mineral exploration*. The Association of Exploration Geochemists Special Volume No. 4. Association of Exploration Geochemists. 93 pages.

– (1974). "Selection of threshold values in geochemical data using probability graphs". *Journal of Geochemical Exploration* 3(2), pages 129–149. DOI: 10.1016/0375-6742(74)90030-2.

Smid, E. and A. Mazot (2012). *Soil gas CO_2 concentrations & CO_2 fluxes in the Auckland Volcanic Field*. Report number 1-2011.02. DOI: 10.17608/k6.auckland.12612461.v1. Institute of Earth Science and Engineering Aotearoa.

Smith, I. E. M. and K. Németh (2017). "Source to surface model of monogenetic volcanism: a critical review". *Geological*

Society, London, Special Publications 446(1), pages 1–28. DOI: 10.1144/sp446.14.

Smith, I. E. M., T. Okada, T. Itaya, and P. M. Black (1993). "Age relationships and tectonic implications of late Cenozoic basaltic volcanism in Northland, New Zealand". *New Zealand Journal of Geology and Geophysics* 36(3), pages 385–393. DOI: 10.1080/00288306.1993.9514583.

Spörli, K. B. and V. R. Eastwood (1997). "Elliptical boundary of an intraplate volcanic field, Auckland, New Zealand". *Journal of Volcanology and Geothermal Research* 79(3–4), pages 169–179. DOI: 10.1016/s0377-0273(97)00030-9.

Spörli, K. B. (1980). *New Zealand and Oblique-Slip Margins: Tectonic Development up to and during the Cainozoic*. DOI: 10.1002/9781444303735.ch9.

Spörli, K. B. and D. Kear, editors (1989). *Geology of Northland: Accretion, allochthons, and arcs at the edge of the New Zealand micro-continent*. Royal Society of New Zealand. 235 pages.

Stix, J. and J. M. de Moor (2018). "Understanding and forecasting phreatic eruptions driven by magmatic degassing". *Earth, Planets and Space* 70(1). DOI: 10.1186/s40623-018-0855-z.

Umeda, K., A. Ninomiya, and T. Negi (2009). "Heat source for an amagmatic hydrothermal system, Noto Peninsula, Central Japan". *Journal of Geophysical Research: Solid Earth* 114(B1). DOI: 10.1029/2008jb005812.

Valley, J. W. (1986). "Stable isotope geochemistry of metamorphic rocks". *Reviews in Mineralogy and Geochemistry* 16(1), pages 445–489.

Viveiros, F., T. Ferreira, J. Cabral Vieira, C. Silva, and J. Gaspar (2008). "Environmental influences on soil CO_2 degassing at Furnas and Fogo volcanoes (São Miguel Island, Azores archipelago)". *Journal of Volcanology and Geothermal Research* 177(4), pages 883–893. DOI: 10.1016/j.jvolgeores.2008.07.005.

Von Veh, M. W. and K. Németh (2009). "An assessment of the alignments of vents based on geostatistical analysis in the Auckland Volcanic Field, New Zealand". *Géomorphologie: relief, processus, environnement* 15(3), pages 175–186. DOI: 10.4000/geomorphologie.7664.

Wallace, L. M., J. Beavan, R. McCaffrey, and D. Darby (2004). "Subduction zone coupling and tectonic block rotations in the North Island, New Zealand". *Journal of Geophysical Research: Solid Earth* 109(B12). DOI: 10.1029/2004jb003241.

Wang, M. and A. Revil (2010). "Electrochemical charge of silica surfaces at high ionic strength in narrow channels". *Journal of Colloid and Interface Science* 343(1), pages 381–386. DOI: 10.1016/j.jcis.2009.11.039.

Weinlich, F., K. Bräuer, H. Kämpf, G. Strauch, J. Tesař, and S. Weise (1999). "An active subcontinental mantle volatile system in the western Eger rift, Central Europe: gas flux, isotopic (He, C, and N) and compositional fingerprints". *Geochimica et Cosmochimica Acta* 63(21), pages 3653–3671. DOI: 10.1016/s0016-7037(99)00187-8.

West Systems (2020). *West Systems portable fluxmeter specifications*. https://www.westgroupnews.com/wp-content/uploads/2016/02/9_Portable.pdf.

Wohletz, K. and G. Heiken (1992). *Volcanology and Geothermal Energy*. Los Alamos Series in Basic and Applied Science No.12. URL: http://ark.cdlib.org/ark:/13030/ft6v19p151/. University of California Press.

Zhao, L., Y. Hu, Y. Zhan, X. Sun, Q. Wang, Y. Zhu, and C. Cao (2022). "Three-dimensional electrical structure and magma system of the monogenetic Longgang Volcanic Field, northeast China, inferred from broadband magnetotelluric data". *Journal of Geophysical Research: Solid Earth* 127(9). DOI: 10.1029/2022jb024694.

Zlotnicki, J., G. Boudon, J. Viodé, J. Delarue, A. Mille, and F. Bruère (1998). "Hydrothermal circulation beneath Mount Pelée inferred by self potential surveying. Structural and tectonic implications". *Journal of Volcanology and Geothermal Research* 84(1–2), pages 73–91. DOI: 10.1016/s0377-0273(98)00030-4.